FOURIER TRANSFORM INFRARED PHOTOACOUSTIC SPECTROSCOPY

By

DENNIS M. DAVIS II

Bachelor of Science

Wichita State University

Wichita, Kansas

1979

Submitted to the Faculty of the
Graduate College of the
Oklahoma State University
in partial fulfillment of
the requirements for
the Degree of
DOCTOR OF PHILOSOPHY
December, 1983

FOURIER TRANSFORM INFRARED PHOTOACOUSTIC SPECTROSCOPY

Thesis Approved:

Thesis Adviser

Dean of Graduate College

ACKNOWLEDGEMENTS

I wish to express my sincere thanks to Dr. Mark G. Rockley, my major advisor, for his guidance and assistance, without which none of this work would have been accomplished. In addition to his guidance and assistance I wish to thank him for putting up with me these last few years. I also wish to express my appreciation to the other committee members, Dr. Lionel M. Raff, Dr. Neil Purdie, and Dr. Richard C. Powell, for their help and participation. Thanks are extended to the entire faculty and staff of the Chemistry Department, particularly Dr. Gil J. Mains, Dr. J. Paul Devlin and Gary Ritzhaupt for their support, friendship, and help through my years at Oklahoma State.

My sincere thanks are extended to the graduate students who befriended me. Among them are: Dr. Dada Najjar, Dr. Joe Sabol, Dr. Bob Kroutil, Roy Pickering, Mark Woodard, Monte Marshall, Heidi Choney, Jim Diers, Monica Wysocki, Charlie Smith, and Randy Turner. There are others, too numerous to mention, so Thank You all.

A note of thanks are also extended to Traci Hershfeld and Dianne Bishop for typing all the drafts of this manuscript. In addition, I wish to thank the Department of the Army for funding the research work in this study.

TABLE OF CONTENTS

LIST OF TABLES

LIST OF FIGURES

CHAPTER I

INTRODUCTION

Background

Over the years, several techniques have been developed which permit the optical investigation of highly light-scattering or opaque materials. The most common of these techniques are diffuse reflectance, attenuated total reflectance (ATR), internal reflection spectroscopy, Raman scattering, and photoacoustic spectroscopy (PAS) (1-4). The techniques of diffuse reflectance, attenuated total reflectance, internal reflection, and Raman scattering are all useful techniques, but each suffers from limitations. In particular, each technique is applicable to only a small category of materials, and each is useful over only a small wavelength range. The last technique, photoacoustic spectroscopy, was developed to study those samples which are unsuitable for study by the conventional transmission and reflection techniques.

In photoacoustic spectroscopy, the sample to be studied is placed in a closed chamber or cell. When studying solids, the sample fills only a portion of the chamber, while the remaining portion is filled with a nonabsorbing gas such as air. At the side of the chamber is a sensitive microphone which is connected to the sample chamber by a small opening. This constitutes a completely sealed arrangement, as shown in Figure 1. The sample is then irradiated by monochromatic light, in the case of dispersive spectrometers, or by a beam of polychromatic light,

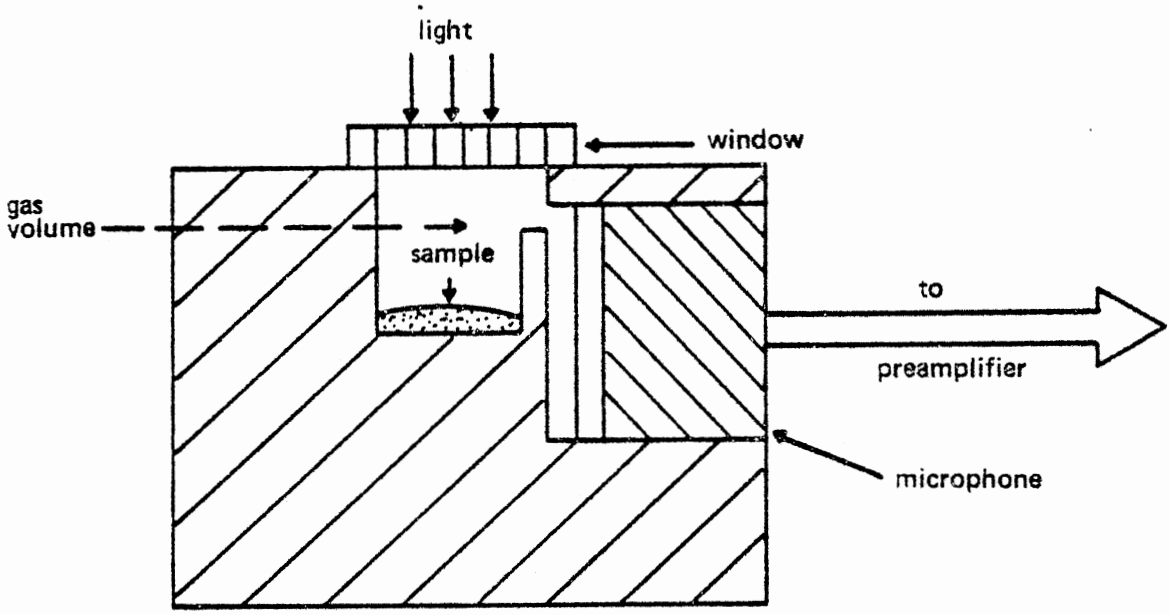

Figure 1. A Simple Photoacoustic Cell

if the instrument being used for the investigation has Fourier Transform capabilities. This light is passed through a mechanical chopper, or is modulated by some other means, such that the beam is amplitude modulated. If any of the light which strikes the surface of the sample is absorbed, internal energy levels within the sample are excited. The subsequent de-excitation of the sample results in the release of the absorbed energy. All or part of this energy is then transformed into heat through non-radiative processes. Since the incident light is intensity modulated, the heating of the sample is also modulated. This heat, when released into the gas in the closed chamber, causes the gas to expand. This expansion causes pressure changes in the chamber which are detected by the microphone.

There are several advantages to photoacoustic spectroscopy. Since the absorption of light is required for the generation of a photoacoustic effect, transmitted light and light scattered by the sample is not detected unless the light is absorbed by the cell walls or strikes the microphone. Hence, transmitted and scattered light do not interfere with photoacoustic measurements. Scattered light, although not directly measured, leads to signal-enhancement effects. These effects make it possible to study highly light-scattering samples such as powders, suspensions and amorphous solids. Another advantage is the capability of obtaining optical absorption spectra on opaque materials, i.e. samples in which no light is transmitted. The last major advantage is that photoacoustic spectroscopy is a non-destructive technique which can be used for performing depth-profiling analysis on the absorptivity of a sample.

Photoacoustic spectroscopy had its beginning in 1880, when

Alexander Graham Bell discovered the photoacoustic effect in both gaseous and nongaseous materials. In his paper to the American Association for the Advancement of Science, Bell (5) briefly reported the accidental discovery of the photoacoustic effect in solids, along with his work on the photophone. The apparatus used by Bell consisted of a voice-activated mirror, a selenium cell, and an electrical telephone receiver. A beam of sunlight was intensity modulated by means of the voice-activated mirror. This modulated beam of light was then focused onto a selenium cell which had been incorporated into a conventional telephone circuit. The electrical resistance of the selenium cell varied with the intensity of the light. Thus, the voice-modulated beam of sunlight resulted in electrically reproduced telephonic speech.

During his experimentation with the photophone, Bell discovered that it was possible to obtain audible signals directly. This could be accomplished if the beam of sunlight was rapidly interrupted and then focused on solid substances which were connected to a hearing tube. Further investigations showed that if a solid material was placed inside a closed glass tube to which a hearing tube was attached, an audible signal could still be obtained if the material in the tube were illuminated by the rapidly interrupted beam of light. Bell (6, p. 515) noted that "the loudest signals are produced from substances in a loose, porous, spongy condition, and from those that have the darkest or most absorbent colors".

Bell (6) demonstrated that the photoacoustic effect in solids was dependent on the absorption of light and that the strength of the signal was dependent on the amount of incident light absorbed by the material in the cell. He concluded (6, p. 527) that "the nature of the

rays that produce sonorous effects in different substances depends upon the nature of the substances that are exposed to the beam, and that the sounds are in every case due to those rays of the spectrum that are absorbed by the body". Thus, Bell correctly deduced the absorptive dependence of the photoacoustic effect.

In addition to studying the photoacoustic effect in solids, Bell (6) also studied the photoacoustic effect in liquids and gases. He noted that liquids produced only weak signals, but that strong signals were obtained when the cell was filled with light-absorbing gases. In these experiments, the detector was the ear. This was an efficient detector for studying the signals in gases, but was not as efficient for the liquids.

After hearing of Bell's discovery, Tyndall (7) and Roentgen (8) also performed experiments on the photoacoustic effect in gases. Bell (6), Tyndall(7), and Roentgen (8) performed early experiments on gases in which they observed that audible signals were obtained from gases in sealed chambers. They noted that colored gases absorbed visible light, while colorless gases absorbed infrared light. The signal which was produced in the sealed chamber was detected by the ear as sound. The absorption of the light by the sample resulted in pressure fluctuations in the air. These fluctuations had the same frequency as the modulation frequency of the light.

The nature of the photoacoustic effect was fairly well understood for gases in the 1880's, because the basic gas laws were already well known. It was correctly assumed that the gaseous samples absorbed all or part of the modulated beam of light, and thus periodically heated. Since the sample chamber was sealed by a compliant diaphragm, the

periodic heating of the gas resulted in both volume and pressure changes. These changes were then transmitted to the ear, and thus the sound was detected. During this time, only a few experiments were performed on liquids, and no explanation of the photoacoustic effect in liquids was attempted.

Several theories were presented in the nineteenth century to account for the photoacoustic effect in solids. To account for the audible signal produced by dark spongy solids such as lampblack, Bell (6) postulated that:

> When a beam of sunlight falls upon the mass, the particles of lampblack are heated, and consequently expand, causing a contraction of the air-spaces or pores among them. Under these circumstances a pulse of air should be expelled, just as we would squeeze water out of a sponge. The force with which the air is expelled must be greatly increased by the expansion of the air itself, due to contact with the heated particles of lampblack. When the light is cut off, the converse process takes place. The lampblack particles cool and contract, thus enlarging the air-spaces among them, and the enclosed air also becomes cool. Under these circumstances a partial vacuum should be formed among the particles and the outside air would then be absorbed, as water is by a sponge when the pressure of the hand is removed (p. 515).

In the case when the solid is in the form of a flexible membrane or disk, Bell supported the theory of Lord Rayleigh (9) which said that the primary source of the photoacoustic signal of a disk, or membrane was the mechanical vibration of the disk resulting from the uneven heating of the disk when it is struck by a beam of sunlight. These conclusions were only partially correct. The hypotheses of Mercadier and Preece were closer to the modern theory of the photoacoustic effect in solids. Mercadier (10, p. 410) suggested that the sound is due to "vibrating movement determined by the alternate heating and cooling produced by

the intermittent radiations, principally in the gaseous layer adhering to the solid surface hit by these radiation". Preece's theory (11, p. 517) is that the photoacoustic effect "is purely an effect of radiant heat, and it is essentially one due to the changes of volume of vapours or gases produced by the degradation and absorption of this heat in a confined space".

After the initial interest generated by Bell's original work, experimentation with the photoacoustic effect apparently ended. This may have been because the photoacoustic effect was considered to be only a scientific curiosity which had no practical or scientific value. Another explanation may be that the experiments were difficult to perform and quantitate since the detector for the signal was the investigator's ear. Whatever the reason, the photoacoustic effect was not studied again for nearly fifty years.

The reappearance of the photoacoustic effect came with the advent of the microphone. In 1938, Viengerov (12) began using the photoacoustic effect to study the absorption of infrared light by gases and to evaluate the concentrations of gaseous species in mixtures of gases. His sources were blackbody infrared sources, such as Nernst glowers. Viengerov's detector was an electrostatic microphone arrangement with which he could measure the voltage change between two charged capacitive microphones. His measurements were seriously affected by the presence of an unwanted photoacoustic effect in the solid windows of his sample chamber.

A year later, Pfund (13) described a gas analyzer system for measuring the concentrations of carbon monoxide and carbon dioxide. Instead of using a microphone for measuring the photoacoutic signal,

Pfund measured the changes in the gas temperature directly, using a thermopile. This thermopile was shielded from the direct optical radiation, and had a sensitivity which was comparable to that obtained by Viengerov.

The next major improvement in the sensitivity of gas concentration analysis occurred in 1943 when Luft (14) described his gas analyzer. This analyzer employed two photoacoustic cells in a differential arrangement. One cell contained the gas sample to be analyzed, while the other cell contained the same gas mixture minus the species of interest. The microphone output from this arrangement was proportional to the pressure difference between the two cells. This arrangement minimized the unwanted photoacoustic signal due to the cell windows, and marked the first time mixtures of more than two gases could be analyzed.

A new impetus for gaseous photoacoustic spectroscopy was provided by high intensity lasers. Because the photoacoustic signal is proportional to the intensity of the incident light, high intensity lasers have made it possible to study gas mixtures which contain species in very low concentrations. Analysis of gas concentrations in the parts-per-billion range have been reported, using high intensity lasers (15, 16).

Since 1973, the photoacoustic effect with solid samples has been studied, and the development of the technique of photoacoustic spectroscopy for nongaseous samples has occurred. The first investigator of the photoacoustic effect with solids was Rosencwaig (4), whose experiments dealt with two-dimensional solids with weak surface absorption properties. At about this time, Parker (17) made the first attempt to

mathematically develop the photoacoustic effect for solids.

In the course of his experiments with the photoacoustic effect in gases, Parker (17) noticed that a small but measurable signal was produced by his gas cell, even when the gas in his cell did not absorb any light. He explained the sound as being attributable to a thin absorbing layer whose function was to convert light to heat, and then transferring that heat to the gas by thermal conduction. In his analysis, this layer could be either an adsorbed gas layer or the surface layer of his glass windows to his cell. He believed that the signal was due to adsorbed gases, with the primary molecules involved being water. However, his calculations and experiments showed that the water could not have been responsible for a signal of the magnitude he had obtained. Having eliminated adsorbed water as a factor, Parker was left with the assumption that a surface layer of his windows produced the photoacoustic signal. This signal may have been related to the surface conductivity of the glass according to Parker's treatment. The major flaw in Parker's treatment was his assumption that an abnormally large fraction of the incident light was being absorbed by a very small layer of his windows. His assumption explained the results of his experiments, but his treatment could be applied to only a limited number of cases.

A more general theory was developed by Rosencwaig and Gersho (18, 19), and is called the RG Theory. The RG Theory assumes, as Mercadier, Preece, and Parker assumed, that the primary source of the photoacoustic signal is due to a periodic heat flow from the solid to the surrounding gas, as the solid is cyclically heated by the absorption of the chopped light. This theory is applicable to most observed effects in the photoacoustic spectroscopy of solids.

Thermal Diffusion Equations

The Rosencwaig-Gersho Theory (RG Theory) is a one-dimensional analysis of the production of a photoacoustic signal from a sample in a cylindrical cell of diameter D and length L, as shown in Figure 2. In the RG Theory, it is assumed that L is small compared to the wavelength of the acoustic signal, and the pressure changes produced by the generated acoustic signal is detected by the microphone. In the arrangement used for developing the theory, l is the length of the sample, lg is the length of the gas column in the cell, and l_b is the length of the backing material. The backing for the cell is a poor thermal conductor, and it is generally assumed that both the gas and the backing material are not light absorbing. The following parameters are defined by Rosencwaig (20), with only the variable names being changed:

K: thermal conductivity (cal/cm-sec-^{o}C)

p: density (g/cm^3)

C: heat capacity (cal/g-^{o}C)

a'= K/pC: thermal diffusivity (cm^2/sec)

$a = (\omega/2a')^{\frac{1}{2}}$: thermal diffusion coefficient (cm^{-1})

u = 1/a: thermal diffusion length (cm)

where ω is the chopping frequency of the incident light beam in radians per second.

If the light source is sinusoidally chopped and monochromatic, the intensity of the light of wavelength λ incident on the solid is given by

$$I = \tfrac{1}{2} I_0 (1 + \cos\omega t) \qquad (1)$$

where I_0 is the monochromatic light flux of the incident beam. The heat

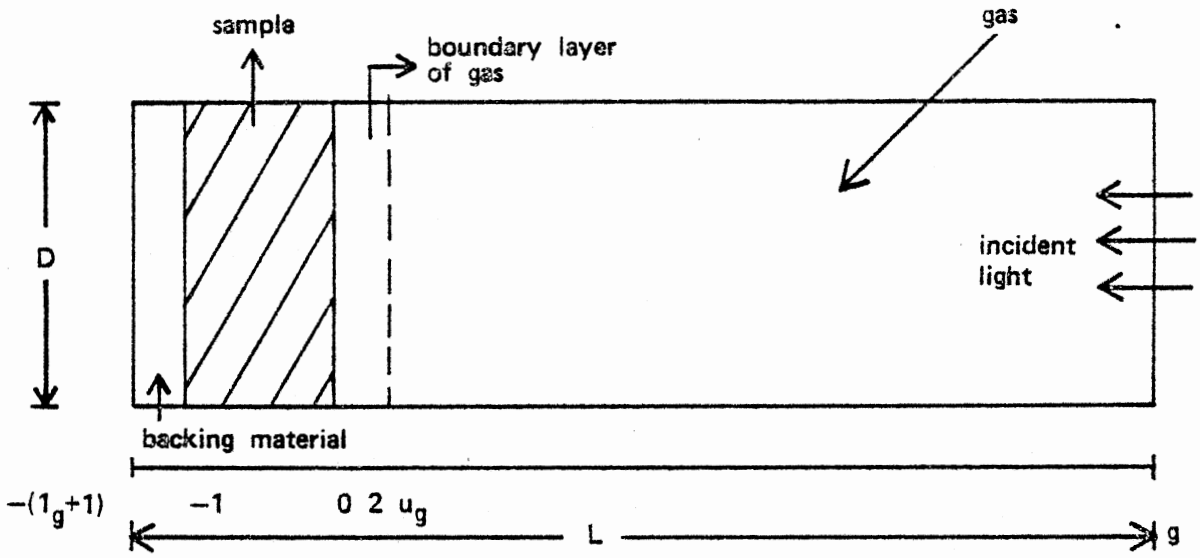

Figure 2. Cross-Sectional View of a Cylindrical PAS Cell (20)

density at any point X due to the light absorbed at this point is

$$\tfrac{1}{2} BI_0 \, \ell^{BX} \, (1 + \cos\omega t) \tag{2}$$

where B is the optical absorption coefficient of the solid sample for wavelength λ, and the values of X range from 0 to $-l$.

Therefore, the thermal diffusion equation for the solid can be written as

$$\frac{\partial^2 \theta}{\partial X^2} = \frac{1}{a'} \frac{\partial \theta}{\partial t} - \frac{BI_0 n}{2K} \ell^{BX} \, (1 + \ell^{i\omega t}) \tag{3}$$

with

$$-l \leq X \leq 0 \tag{4}$$

where θ is the temperature and n is the efficiency at which the light is converted to heat. For most solids at room temperature, it is assumed that n = 1. For the backing, the heat diffusion equation is given by

$$\frac{\partial^2 \theta}{\partial X^2} = \frac{1}{a'_b} \frac{\partial \theta}{\partial t}, \qquad -(l_b + l) \leq X \leq -l \tag{5}$$

and the heat diffusion for the gas is given by

$$\frac{\partial^2 \theta}{\partial X^2} \; \frac{1}{a'_g} \frac{\partial \theta}{\partial t}, \qquad 0 \leq X \leq l_g. \tag{6}$$

The temperature in the cell relative to the ambient temperatures as a function of position and time is given as the real part of the solution of $\theta(x,t)$ for Equations (3)-(6). The temperature of the cell is then given by

$$T(X,t) = \theta'(X,t) + \phi_0 \tag{7}$$

where $\theta'(X,t)$ is the real part of the solution of $\theta(X,t)$ and ϕ_0 is the ambient temperature. The solutions for $\theta(X,t)$ which satisfy the boundary constraints at the interfaces between the various regions of

the cell yield

$$T(0,t) = \phi_0 + F_0 + \theta_1 \mathrm{COS}\omega t - \theta_2 \mathrm{SIN}\omega t \tag{8}$$

where $T(0,t)$ is the temperature of the gas-sample interface as a function of time, F_0 is the increase in temperature due to the absorbed heat and θ_1 and θ_2 determine the in-phase and quadrature components of the periodic temperature variation at the surface X=0 for the sample.

The periodic temperature variation in the gas is given by

$$\theta(X,t) = \theta_0 \ell^{\sigma_g X} \ell^{i\omega t} \tag{9}$$

where θ_0 is the complex amplitude of the periodic temperature at the gas-sample boundary which is given by

$$\theta_0 = \frac{BI_0}{2K(B^2 - \sigma_g^2)} \left[\frac{(r-1)(b+1)\ell^{\sigma_g 1} - (r+1)(b-1)\ell^{\sigma_g 1} + 2(b-r)\ell^{-B1}}{(g+1)(b+1)\ell^{\sigma_g 1} - (g-1)(b-1)\ell^{\sigma_g 1}} \right] \tag{10}$$

where

$$b = \frac{K_b a_b}{K_a} \tag{11}$$

$$g = \frac{K_g a_g}{K_a} \tag{12}$$

and

$$r = (1-i)\frac{B}{2a} \tag{13}$$

with $\sigma_g = (1+i)a$. Taking the real part of Equation (9) yields the actual temperature variation of the gas, which is given by

$$T(X,t) = e^{-a_g X}\left[\theta_1 \mathrm{COS}(\omega t - a_g X) - \theta_2 \mathrm{SIN}(\omega t - a_g X)\right], \tag{14}$$

where θ_1 and θ_2 are the real and imaginary parts of θ_0 respectively. At a distance $2\pi U_g$, where U_g is the thermal diffusion length of the gas, the periodic temperature variation is essentially equal to zero. This defines a boundary layer of gas whose thickness is $2\pi U_g$. This layer of the gas is, to a good approximation, the only portion of the gas which is capable of thermally responding to the periodic temperature changes

at the sample interface.

The average temperature of this layer is found by evaluating

$$<\theta(t)> = \frac{1}{2\pi U_g} \int_0^{2\pi U_g} \theta\,(X,t)dx. \tag{15}$$

Evaluation of this integral yields

$$<\theta(t)> = \frac{1}{2\pi\sqrt{2}}\,\theta_o e^{i(\omega t - \frac{\pi}{4})} \tag{16}$$

if we assume $e^{-2\pi} << 1$.

The periodic heating of the boundary layer causes this layer to periodically expand and contract. This expansion and contraction acts as a thermal piston which works on the rest of the gas column. If the ideal gas law is used, the displacement of the gas piston due to the periodic heating can be estimated by

$$\delta X(t) = 2\pi U_g \frac{<\theta\,(t)>}{T_o} \tag{17}$$

where $<\theta(t)>$ is a defined by Equation (16), and T_o is the average temperature of the gas boundary layer such that $T_o = \emptyset_o + F_o$.

If the rest of the gas layer responds adiabatically, the incremental pressure is

$$\delta P\,(t) = \frac{\gamma P_o}{l_g}\,\delta X\,(t) \tag{18}$$

where P_o is the ambient pressure, and γ is the ratio of the heat capacities of the gas. If Equations (17) and (18) are combined, the resulting expression is

$$\delta P(t) = \frac{\gamma P_o\,\theta_o}{a g l_g T_o \sqrt{2}}\,e^{i(\omega t - \frac{\pi}{4})} \tag{19}$$

Thus the actual pressure variation, $\Delta p(t)$, is given by

$$\Delta p(t) = Q_1 \cos(\omega t - \frac{\pi}{4}) - Q_2 \sin(\omega t - \frac{\pi}{4}) \tag{20}$$

where Q_1 and Q_2 are the real and imaginary parts of Q, the envelope of the sinusoidal pressure variation which is given by

$$Q = \frac{BI_0 \gamma P_0}{2\sqrt{2}\, T_0 K l g a_g (B^2 - \sigma g^2)}$$

$$\times \frac{(r-1)(b+1)e^{\sigma g l} - (r+1)(b-1)e^{-\sigma g l} + 2(b-r)e^{-B l}}{(g+1)(b+1)e^{\sigma g l} - (g-1)(b-1)e^{-\sigma g l}} \tag{21}$$

At ordinary temperatures $T_0 \cong \emptyset_0$ so that the temperature distribution does not need to be evaluated, and Equation (21) can be evaluated for the magnitude and phase of the acoustic pressure wave which is produced in the cell by the photoacoustic effect.

In an effort to gain insight into the physical meaning of Equation (21), Rosencwaig (20) discusses six special cases for the application of the RG Theory. Only five cases will be presented because two of the cases give degenerate answers. The first of these cases deals with optically transparent, thermally thin solids, which is the degenerate case. For solids of this type, light is absorbed throughout the sample, and the heat generated by the entire sample and the backing is measured, and Q becomes

$$Q = \frac{Y}{2 \ddot{a}_g a_b K_b} (B - 2\ddot{a}b - iB) \cong \frac{(1-i)B}{2a_g} \left(\frac{U_b}{K_b}\right) Y \tag{22}$$

where

$$Y = \frac{P_0 \gamma I_0}{T_0 l_g 2\sqrt{2}} \tag{23}$$

Thus, the acoustic signal is proportional to Bl which means the acoustic signal is inversely proportional to the chopping frequency. The signal is

also proportional to the thermal properties of the backing material.

The second case is for optically transparent, thermally thick solids. For solids with these characteristics, the expression for Q becomes

$$Q \cong -i \frac{Bu}{2a_g} \left(\frac{u}{K}\right) \quad Y \tag{24}$$

In this case, the acoustic signal is proportional to Bu. This means that only the light which is absorbed by the first diffusion length of the sample contributes to signal, even though light may be absorbed throughout the sample.

These two cases, which deal with optically transparent solids, demonstrate the capability of using photoacoustic spectroscopy for depth profiling the optical absorption spectra of solids. To accomplish this, one must simply alter the chopping frequency of the light. This will cause a change in the thermal diffusion length of the solid, and the changes in the spectra can then be monitored.

The next three cases deal with solids which are optically thick, that is most of the light is absorbed at a distance which is small compared to l. In these cases, virtually no light is transmitted through the sample. The first case for samples of this type are thermally thin solids where $u>>l$ and $u>>\frac{1}{\beta}$. For these solids, the

$$Q \cong \frac{(1-i)}{2a_g} \left(\frac{u_b}{K_b}\right) Y. \tag{25}$$

In this case, the acoustic signal is independent of B. An example of a solid which fits into this category is carbon black, a reference in many photoacoustic experiments. From Equation (25) it is seen that the signal strength varies inversely with ω, and is dependent upon the thermal properties of the backing material.

The next case deals with optically thick, thermally thin solids where $u < \ell$ and $u > l_B$. For these solids, Q is given by

$$Q \cong \frac{(1-i)}{2a_g} \left(\frac{u}{K}\right) Y. \tag{26}$$

Here, the signal is inversely proportional to ω, but the intensity of the signal is no longer dependent upon the thermal properties of the backing. Instead, the signal intensity is dependent upon the thermal properties of the sample.

The last special case deals with solids which are optically thick, and thermally thick. Here, Q is given by

$$Q \cong \frac{-B\ u\ i}{2a_g} \left(\frac{u}{K}\right) Y. \tag{27}$$

In this case, the signal is dependent upon the thermal properties of the sample, with only the light absorbed in the first thermal diffusion length contributing to the signal. The signal in this case is proportional to B, but it is inversely proportional to $\omega^{3/2}$.

In general terms, this theory shows that the generation of the pressure fluctuation in the cell is dependent upon the acoustic pressure disturbance at the gas-sample interface and the subsequent propagation of this signal to the microphone. The acoustic pressure disturbance can be compared to a thermal piston. This piston moves as a function of the periodic heat flow from the sample to the gas. This thermal piston then creates an acoustical shock wave which is detected by the microphone.

Refinements in the RG Theory have been made by Aamodt, et al., Bennett and Forman, and Wetsel and McDonald (21-23). The analysis performed by Wetsel and McDonald considered the contributions to the photoacoustic signal from thermally induced mechanical vibrations of

the sample. Their analysis follows the same treatment as that of Rosencwaig and Gersho, but is a little more complicated. The results of the two treatments, the RG Theory and the Wetsel and McDonald model, are essentially identical. Thus, either approach appears to be applicable to the analysis of the photoacoustic phenomenon.

In the 1970's, much of the work in photoacoustic spectroscopy was performed in the visible and ultraviolet regions of the electromagnetic spectrum. In these regions, the photoacoustic spectra which were obtained often exhibited broad, structureless features. When this shortcoming of the PAS spectra in the ultraviolet-visible region is combined with the knowledge that the vibrational spectra of compounds occur in the mid-infrared region, it becomes apparent that photoacoustic spectroscopy needs to be extended into the mid-infrared region. However, the broadband infrared sources are generally too weak to be used with conventional monochromators. This problem was overcome in the visible range in 1978 when Farrow, et al. (24-26), developed a technique known as Fourier Transform Photoacoustic Spectroscopy. In their technique, Farrow and coworkers employed a Michelson interferometer. A Michelson interferometer has two advantages over conventional monochromators. The first advantage, known as Fellget's advantage, is that the data are collected at all spectral frequencies simultaneously, which allows a higher signal to noise ratio than is available with a conventional monochromator. The second advantage, Jacquinot's advantage, allows a much higher optical throughput. A schematic of the experimental arrangement used by Farrow and coworkers is shown in Figure 3.

In the Michelson interferometer, the intensity of the beam at the detector is determined as a function of the difference between the two

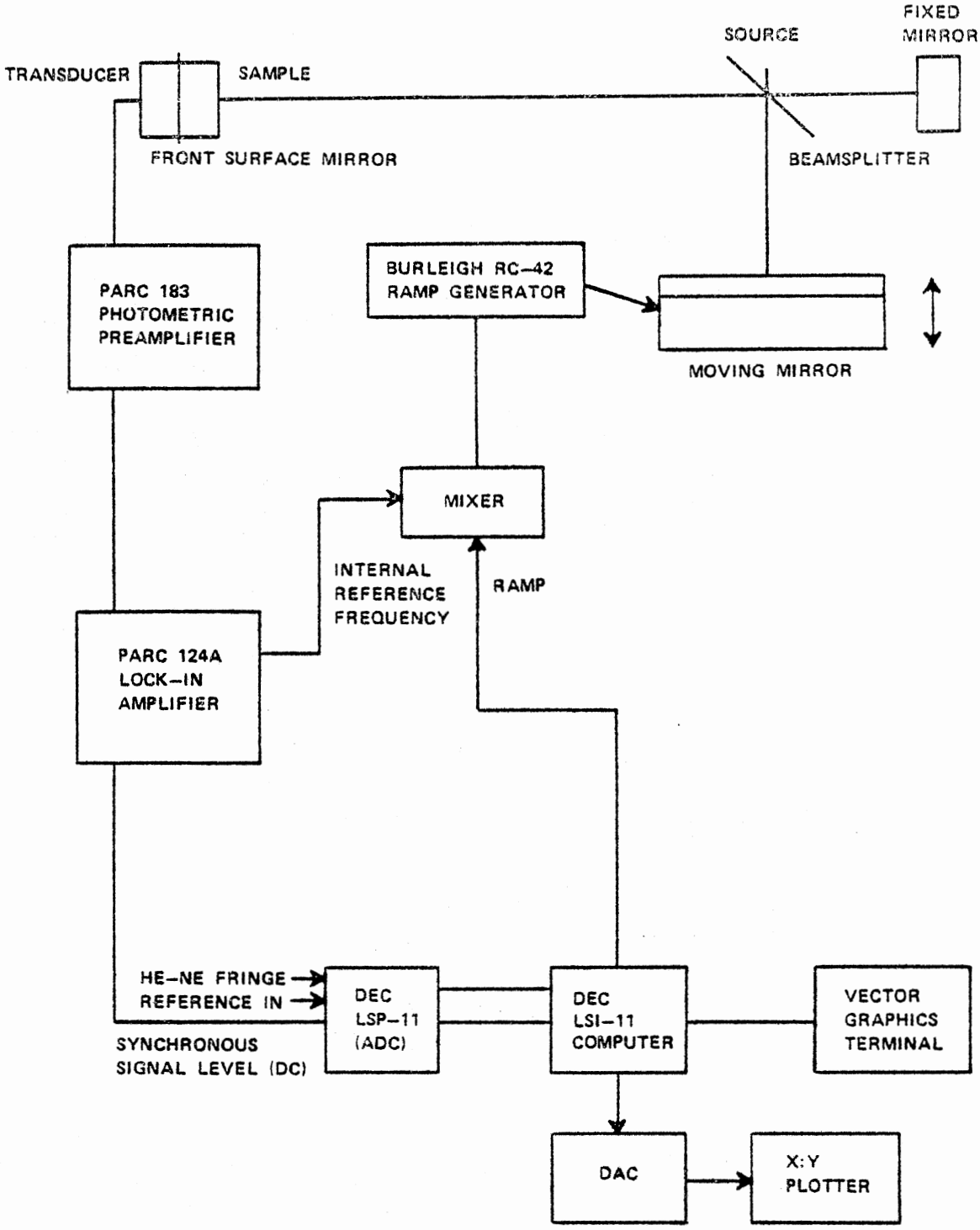

Figure 3. Schematic of Farrow's (24) FT Spectrometer

mirrors of the interferometer. The optical path difference, x, between the beams traveling between the fixed and moveable mirrors is given by

$$X = 2\ (M_1 - M_2) \tag{28}$$

where M_1 is the distance to the moveable mirror, and M_2 is the distance to the fixed mirror. Whenever $x = \lambda n$, where λ is the frequency of light, the two beams are in phase and give a maximum intensity at the detector. If $x = n\ \lambda/2$, where n is an odd integer, the two beams are 180 degrees out of phase and destructively interfere upon recombination, thus giving a minimum at the detector.

If the intensity of the signal is measured as the mirror is moved at a constant velocity V, it will vary sinusoidally with a frequency given by

$$f = 2Vs \tag{29}$$

where f is the heterodyne frequency of the spectral frequency s, and $s = 1/\lambda$. Thus, the intensity can be measured as a function of the optical path difference. This intensity, I(x) is given by

$$I(x) = B(s)\left[1+\cos(2\pi xs)\right] \tag{30}$$

where B(s) is the spectral intensity of wavenumber s. The intensity I(X) is said to be the Fourier cosine transform of B(s), the desired spectral intensity. Thus, for the case where B(s) represents a continuum of spectral intensities, the interferogram is given by

$$I(x) = \int_0^\infty B(s) \cos\ (2\pi Xs)\ dS. \tag{31}$$

Using the Fourier inversion theorem, an expression for B(s) may be obtained. The expression for B(s) is given by

$$B(s) = \int_0^\infty I(x) \cos\ (2\pi Xs)\ dX. \tag{32}$$

At about this same time, Busse and Bullemer (27) demonstrated that a Fourier Transform Infrared Spectrometer could be used to measure the

infrared photoacoustic spectrum of gases in a spectrophone, and Low and Parodi (28,29) demonstrated that it was possible to perform PAS surface studies using a conventional infrared source and a dispersive spectrometer. Of the two, the work of Low and Parodi is the more important as it was the first PAS work performed in the infrared region using conventional equipment. In their work, Low and Parodi used a modified Perkin-Elmer dispersive infrared monochromator to obtain the PAS spectra of surface species on silica. In particular, they studied the chemisorption of methanol, as the Si-O bond is very easy to distinguish in the infrared spectrum. Their work was limited to the 3900 to 1400 cm^{-1} range, because their source was not intense enough to study the PAS spectrum in the 1400 to 600 cm^{-1} range. Even though their experiments were only of a preliminary nature and the spectral resolution was poor in comparison to absorption spectra, Low and Parodi demonstrated the potential of this technique.

After these initial experiments, Low and Parodi (30,31) altered their experimental arrangement. Instead of the monochromator, they used a modified Perkin-Elmer 421 infrared spectrometer. This new arrangement was used to study a variety of solids with considerably better spectral resolution. However, Low and Parodi still had problems with their photoacoustic system, particularly the signal strength. Because their signal was weak, they replaced the 421 with a Perkin-Elmer 621. With this, Low and Parodi achieved a much greater signal, but at the expense of the resolution. When they maximized the resolution, they lost the advantage of the increased signal. Hence, with the Low and Parodi arrangements one had to choose between resolution and signal strength.

At the time that Low and Parodi performed their work on photoacoustic

spectroscopy in the mid-infrared region, theirs was the only reported work using conventional infrared instruments. There was other work being done with photoacoustic spectroscopy in the infrared region however. This work was performed by Nordal and Kanstad (32-34). In their work, Nordal and Kanstad used a pulsed, tunable CO_2 laser as a light source. This source emitted a number of discrete lines in the 9.2 - 10.7 micron range.

Nordal and Kanstad studied a variety of systems using both photoacoustic spectroscopy and photoacoustic reflection-absorption spectroscopy (PARAS). The technique they developed, PARAS, revealed an interesting result. They noticed that the choice of windows for the photoacoustic cell is critical in the analysis of PAS spectra. This observation was made when they noticed a shift in the spectra when samples were analyzed using both PARAS and normal photoacoustic spectroscopy.

Using the techniques of Nordal and Kanstad, it was possible to obtain the infrared spectra of compounds below the 3900 to 1400 cm^{-1} range. There were, however, limitations to their techniques. The main limitation is the lack of broadband laser sources in the infrared range. For this reason, the amount of data which could be obtained was limited. Nordal and Kanstad had demonstrated the usefulness of photoacoustic spectroscopy in the mid-infrared range, but they also pointed out its limitations.

Even with these advances, the application of photoacoustic spectroscopy in the infrared region was incomplete. Using the technique of Low and Parodi, it was possible to measure the photoacoustic spectra of solids down to around 1400 cm^{-1}, but to go any farther required the

use of CO_2 lasers (32). Still the spectral resolution was generally poor and the spectra had low signal to noise ratios. Thus, there was still a need for improving the technique in the infrared region. This improvement was made in the late 1970's when Rockley (35-38) combined the techniques of Farrow and coworkers and Low and Parodi. The new technique is called Fourier Transform Infrared Photoacoustic Spectroscopy (FTIR-PAS).

In the development of FTIR-PAS, a Digilab FTS-20 Fourier Transform Infrared Spectrometer was used. The advantages of this technique were that the light throughput of the FTS-20 was about fifty times greater than that of dispersive instruments, and the multiplexing advantage of the Fourier Spectrometer could be utilized. The higher light throughput made it possible to obtain photoacoustic spectra in the entire mid-infrared region. The multiplexing advantage enabled him to record these spectra with good spectral resolution, as his apparatus was not limited by the signal strength at the detector.

At about the same time as these papers appeared in the literature, Vidrine (39) also proposed the technique using a Nicolet 7199A FT-IR. In his work, Vidrine modified the mirror velocity of his spectrometer to lower the possibility of signal saturation, and to maximize the signal-to-noise ratio. Vidrine examined the utility of Fourier Transform Infrared Photoacoustic Spectroscopy in the analysis of polyurethane feedstock, analgesic tablets, liquids, and plastics and found that the technique was applicable to all types of solids, regardless of the porosity, shape or texture of the surface.

In their work, both Rockley and Vidrine reported the advantages of using Fourier Transform Photoacoustic detection of solids in the infrared.

Among these advantages are the ability to study samples of various textures, minimum sample preparation, high signal-to-noise ratios, and the ease with which the spectra could be obtained. Thus, Fourier Transform Infrared Photoacoustic Spectroscopy should be a useful tool in the analysis of solid samples.

Statement of Problem

With the introduction of Fourier-Transform Infrared Photoacoustic Spectroscopy, it became possible to study the infrared spectra of solid samples with little or no sample preparation. The spectra could be measured without making a potassium bromide pellet, or dissolving the solid in a solvent, techniques which could alter the spectra or contaminate the sample. Thus, the technique provides a nondestructive means of studying the solid samples.

The content of this thesis describes some preliminary applications of FTIR-PAS. It shows the range of usefulness of this technique, through its application to biological materials and inorganic compounds. It also demonstrates the first attempts at using FTIR-PAS for the quantitative analysis of solid mixtures, quantization of the signal with respect to particle size, and the application of the technique for analyzing amorphous carbon surfaces.

CHAPTER II

EXPERIMENTAL

All Fourier Transform Infrared Photoacoustic spectra were recorded on a Digilab FTS-20C spectrometer using a resolution of 8 cm^{-1}. The output from the interferometer head was reflected into the photoacoustic cell by a front surface mirror whose angle of interception of the beam was 45°. To remove atmospheric water from the photoacoustic cell, a small pan containing freshly regenerated molecular sieves was placed at the bottom of the sample chamber. These sieves were isolated from the incident beam by a sheet of aluminum foil. This arrangement provided no signal unless a sample was placed in the chamber.

Photoacoustic Cells and Arrangement

The photoacoustic cell which was used for studying the biological materials, quantization with respect to particle size, and quantitative analysis of an isotopic mixture of potassium nitrate was different from the cell used to study the carbon surfaces and drugs. For the biological materials, particle size and isotopic mixtures, the sample cell has a volume of 1 cm^3 and is sealed with a sodium chloride window. In one side of this cell is an air conduit of 2 millimeter diameter and 2 centimeter length. At the other end of this conduit is a GR1962 1/2 inch foil electret microphone (from General Radio). The signal from this microphone is amplified by 10 with an Ithaco 143L preamplifier and is further amplified by a broadband amplifier by another factor of 10.

This sample cell is then placed in the sample compartment of the Digilab FTS-20C spectrometer which has an evacuable interferometer head. The infrared beam from the interferometer head is then deflected vertically by a front surface mirror and focused with an f/1 cesium iodide lens into the sample chamber of the PAS cell. The output of the microphone is then connected to the signal processing electronics of the FTS-20 spectrometer. The spectra of the different samples are then recorded using the standard software supplied with the FTS-20 spectrometer. A schematic is shown in Figure 4.

After these initial studies, it was decided that the photoacoustic cell assembly needed to be changed. The reasons for this change were two-fold. First, this cell used silicon grease for a seal. This grease had a tendency to adhere to the entrance window of the cell and subsequently produced an unwanted signal. The second reason was the necessity of enhancing the signal-to-noise ratio. To overcome these problems, a greaseless PAS cell was developed. The mechanical drawings for this cell are shown in Figures 5 through 9.

The new cell consists of a set of matching photoacoustic cells which are machined out of aluminum and lined with stainless sleeves. The sample chambers for these cells are sealed with 3 millimeter thick NaCl windows. One of these cells is left empty, while the other one is used as a sample chamber. Each cell uses a Bruel and Kjaer 1/2 inch foil electret microphone model 4175. The response of each microphone is 50 millivolts per microbar. The output of these two microphones are then connected to Bruel and Kjaer model 2642 preamplifiers and a Bruel and Kjaer model 2810 power supply. The output of the power supply is then passed into a differential amplifier which substracts the signal

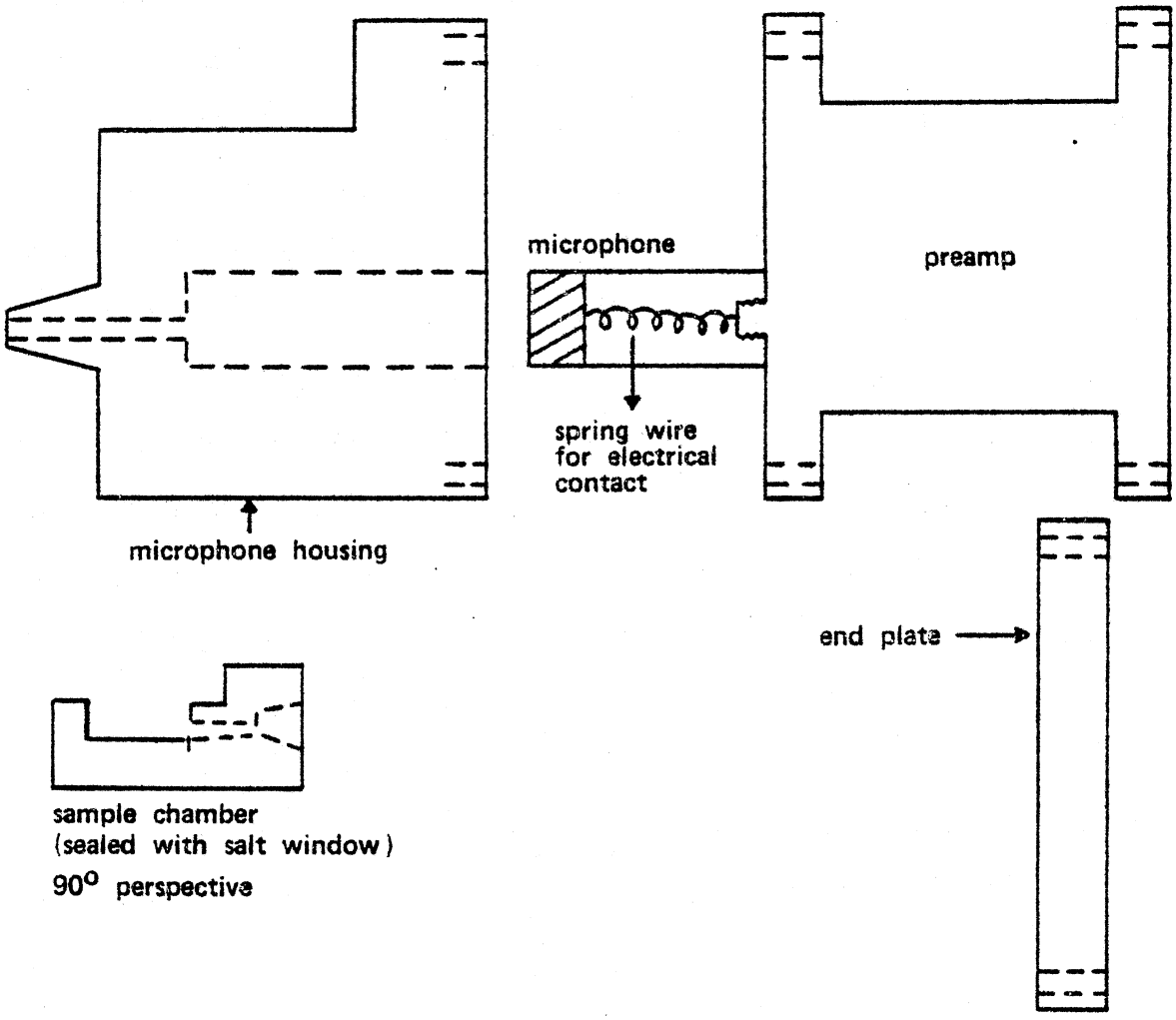

Figure 4. Greased Cell

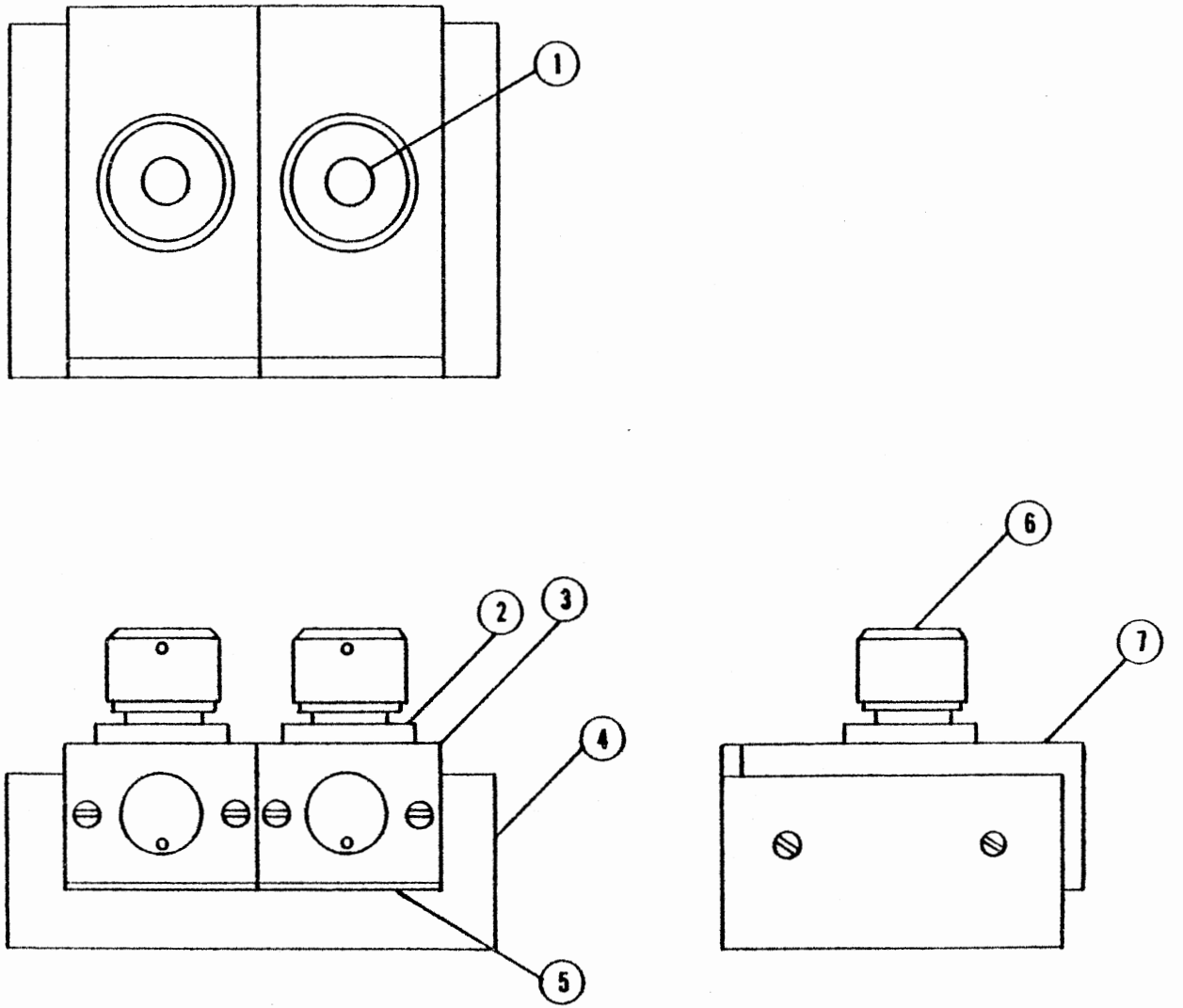

Figure 5. Detailed Mechanical Drawing of Photoacoustic Cell Assembly

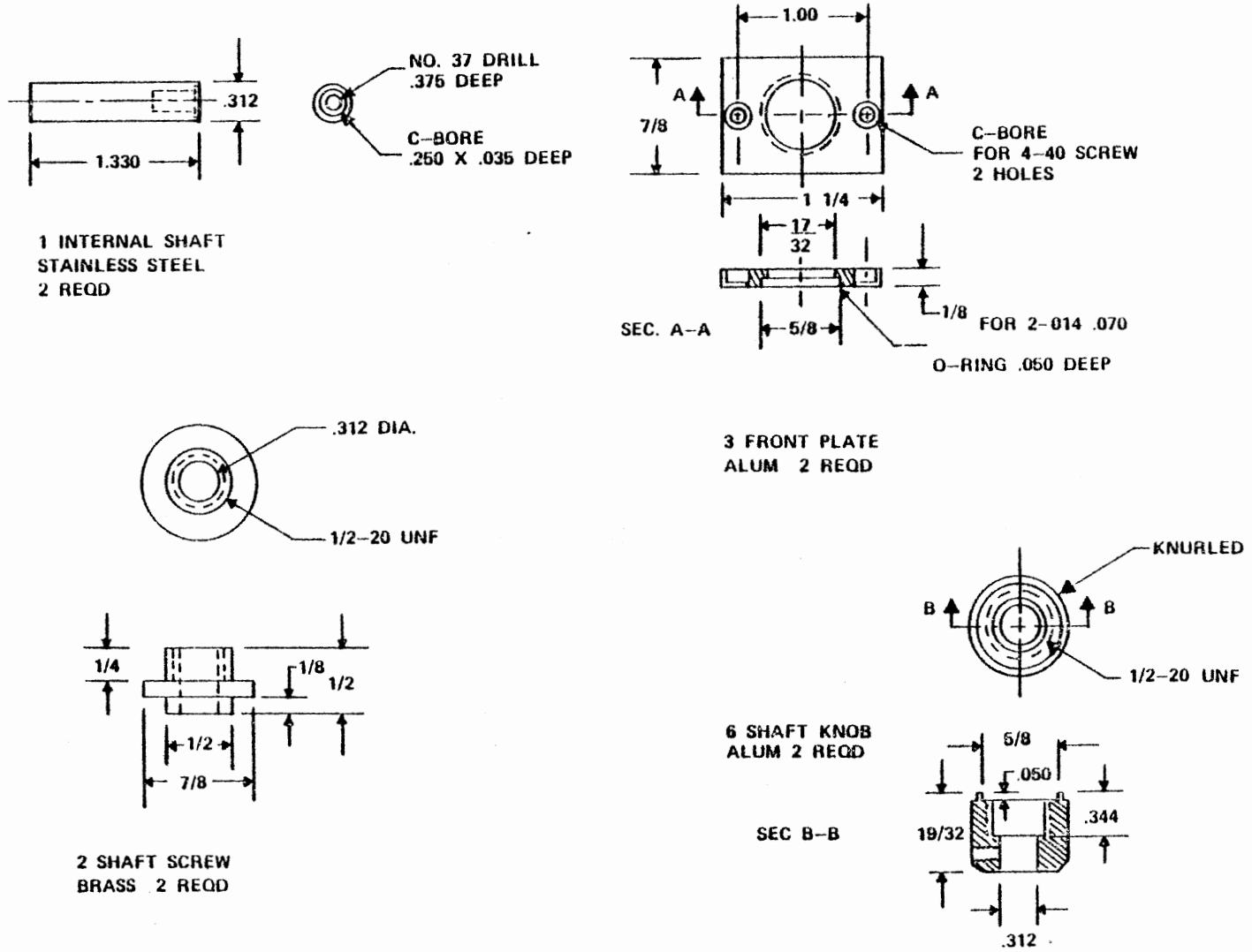

Figure 6. Detailed Mechanical Drawing of Photoacoustic Cell

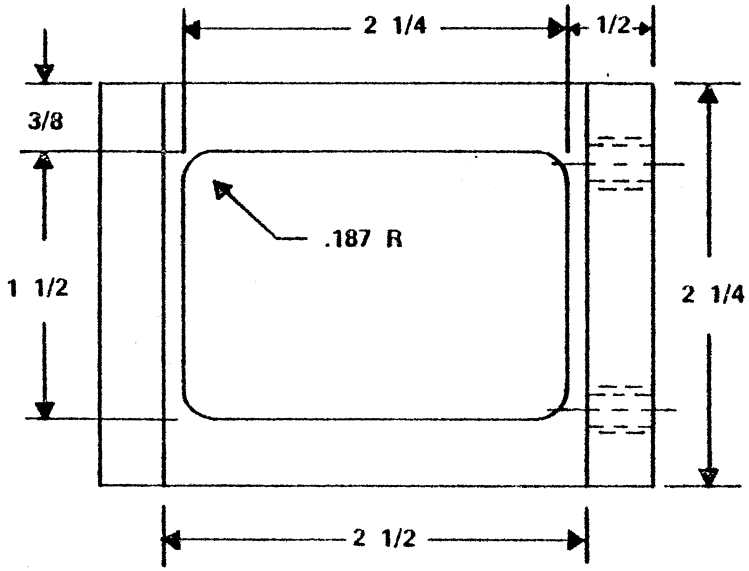

4 HOLDING BRACKET
ALUM 1 REQD

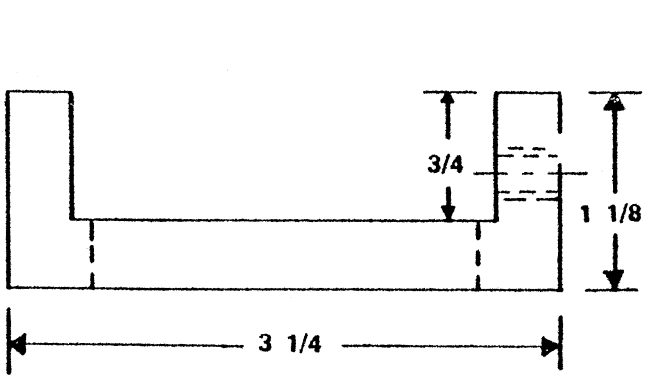

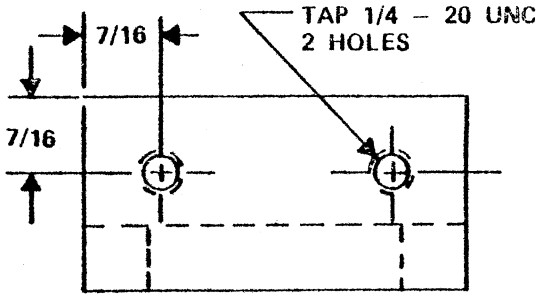

Figure 7. Detailed Mechnical Drawing of Photoacoustic Cell

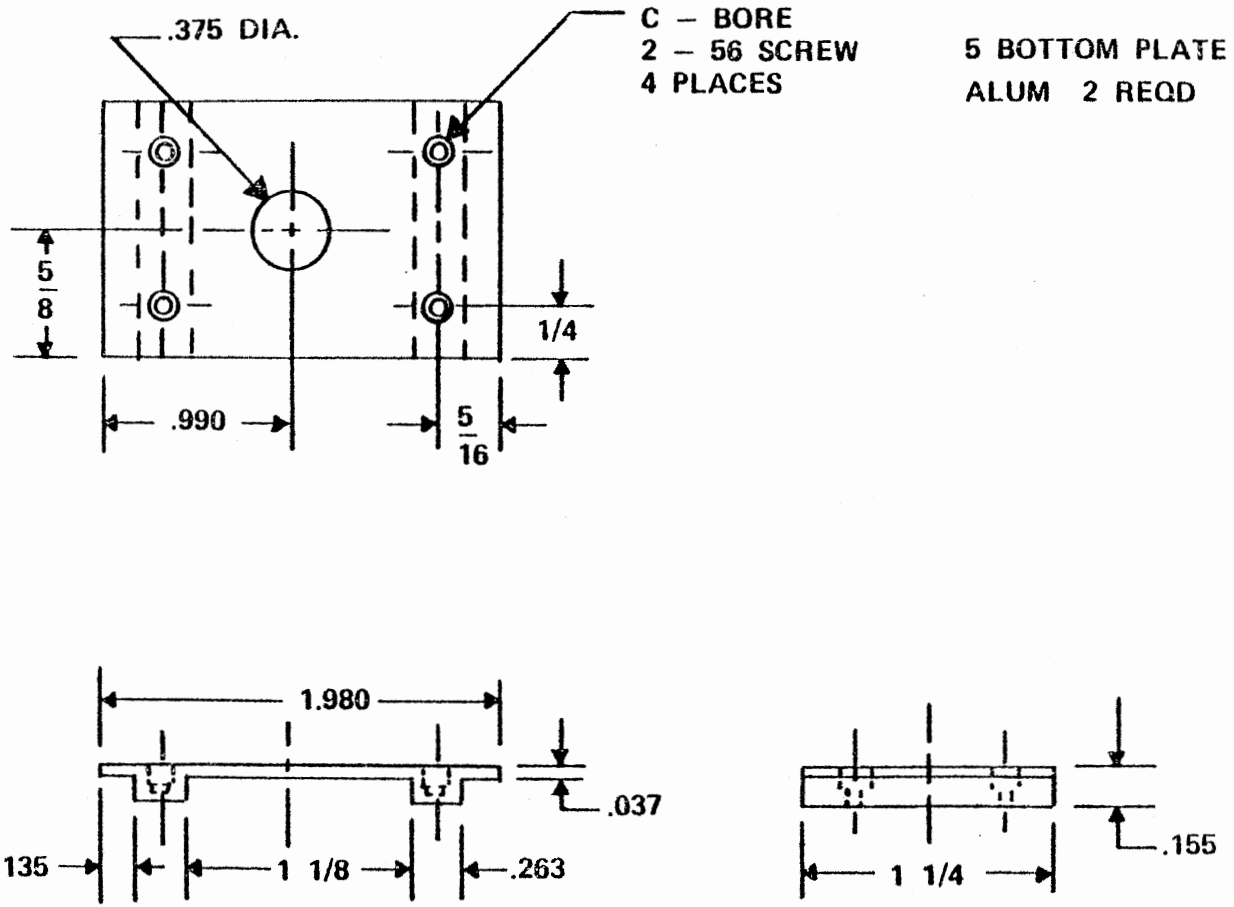

Figure 8. Detailed Mechanical Drawing of Photoacoustic Cell

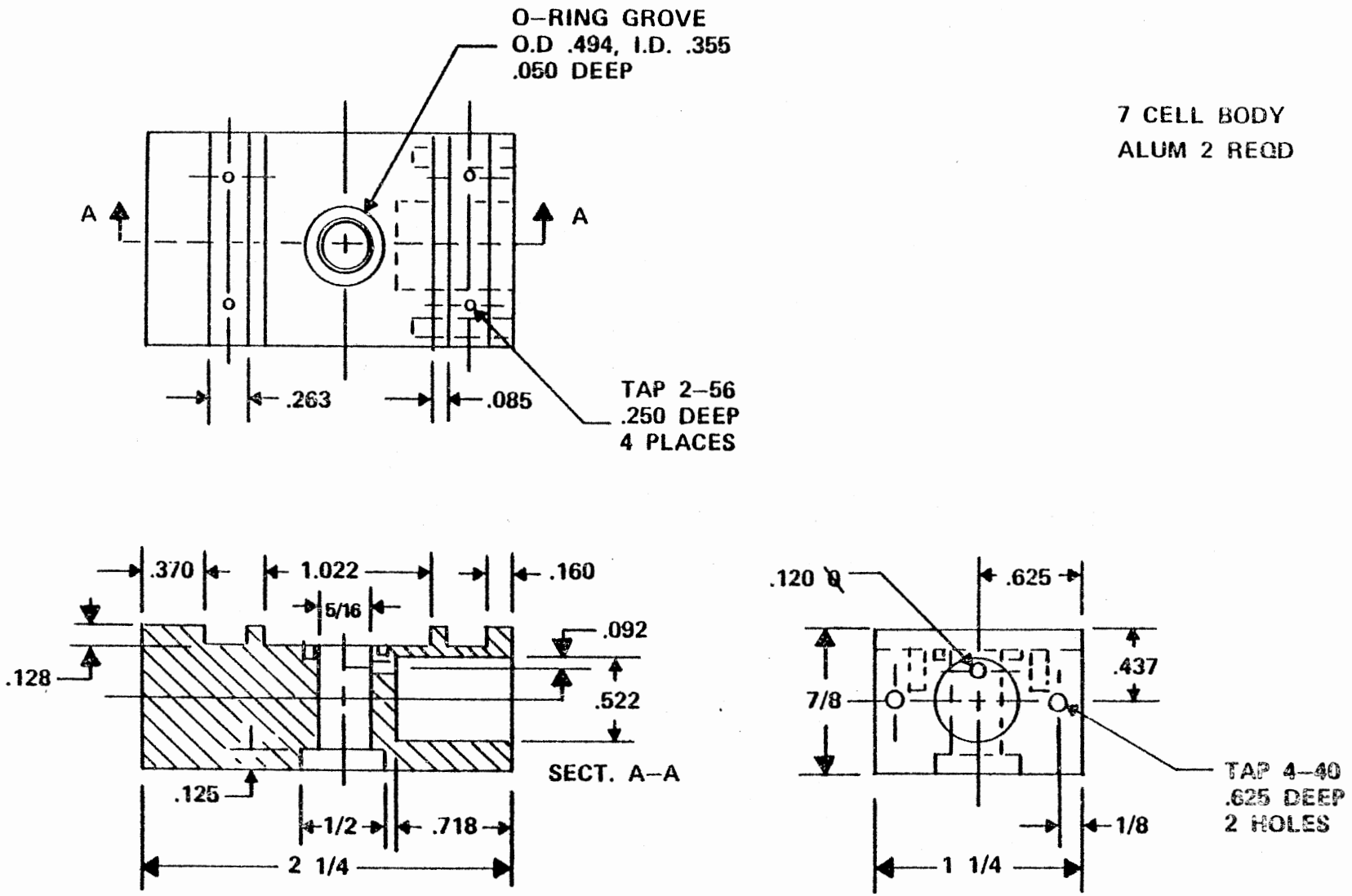

Figure 9. Detailed Mechanical Drawing of Photoacoustic Cell

of the empty cell from the signal of the sample cell. The settings of the differential amplifier were maximized for carbon black and remained constant thereafter. The maximized setting gave the highest signal-to-noise ratio for the carbon black sample. The output of the differential amplifier is then connected to the signal processing electronics of the FTS-20 spectrometer and the spectra are recorded.

After the new cells were produced, it was necessary to characterize their response. This was done by using two separate techniques. The first technique, or step, is to adjust the differential amplifier such that the percent noise is minimized. This may be accomplished by alternately adjusting the potentiometers of the differential amplifier and running a 100% line on the spectrometer. Lampblack (or charcoal) is used to maximize the signal, and 20 scans are run for such a test. After adjustment, the lowest percent noise obtained on a lampblack sample was approximately 0.2 - 0.4%. Once the settings on the differential amplifier were set to maximize the signal-to-noise ratio (SNR or S/N Ratio), or alternately to minimize the percent noise, it was necessary to measure the response of the cells vs. frequency. This was done by measuring the Signal versus Modulation Frequency. The procedure for these measurements is as follows:

1. Turn on HeNe laser and lock-in amplifier and allow them to warm ~~up~~.
2. Turn on frequency meter and mechanical chopper.
3. Set chopper to desired frequency and allow it to stabilize.
4. Measure the signal intensity in millivolts by:
    a. Deflecting laser beam into sample chamber,
    b. Turning microphone power supply on,

c. Adjusting the phase until meter reads zero,

d. Flip the lock-in amplifier to 90 degrees out of phase and read signal.

5. Measure noise in millivolts by:

a. Blocking the laser beam with an aluminum block,

b. Reading the maximum total deflection of the needle on the lock-in amplifier while using the lowest possible settings of the sensitivity.

Example: A deflection of 0.02 mV in the negative direction and 0.01 mV in the positive direction result in a noise level of 0.03 mV.

The data for the two cells, arbitrarily named the Right-Hand-Cell and Left-Hand-Cell gives the signal response, S, in millivolts, and the signal-to-noise ratio, SNR, with respect to the frequency of the chopper f, or logrithm of f, for the Right-Hand-Cell and Left-Hand when no differential amplifier is used. This information is shown graphically in Figures 10-17. It should be noted that slopes of the lines in Figures 10-17 range from of low of (-1.047) to a high of (-0.970). These values show the frequency response of the carbon black to be of the order W^{-1}, where W is the frequency, while RG Theory predicts the response to be of the order $W^{-3/2}$. This apparent discrepancy has recently been addressed by Rosencwaig (40). In loosely packed carbon black, most of the internal volume of the carbon is the gas of the chamber. Since thermal contact with other particles occurs only at points of physical contact between particles, most of the effective backing for the carbon is the gas. Thus, RG Theory would yield the result that the frequency dependence varies as W^{-1}. Figures 15-17 are plots of the signal-to-noise ratio versus the chopping frequency. The

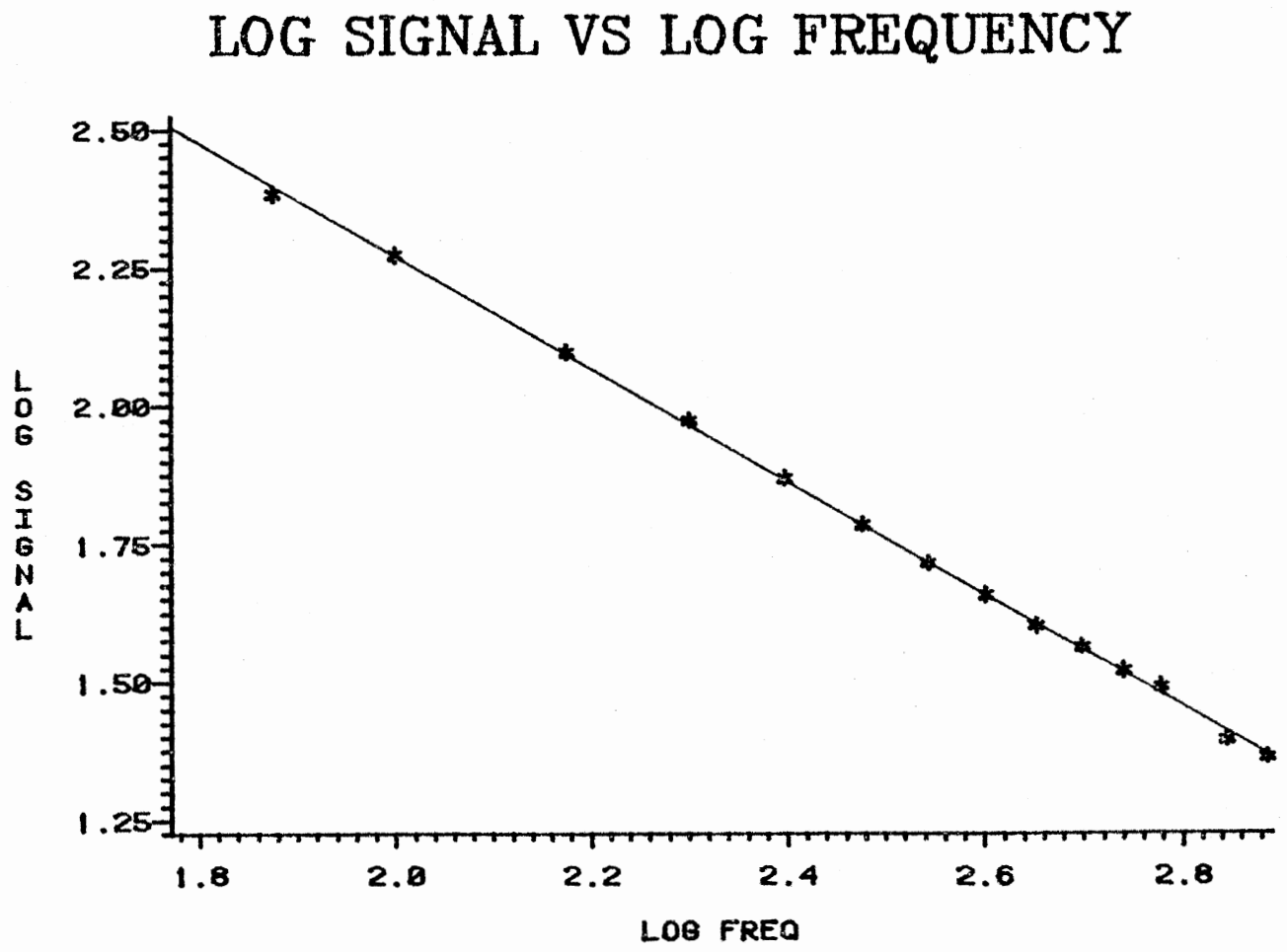

Figure 10. Plot of Signal vs. Log Frequency for the Left-Hand-Cell of the Differential Amplifier Arrangement. No Differential Amplifier is Used. The Slope is -1-.025. The Sample is Carbon Black

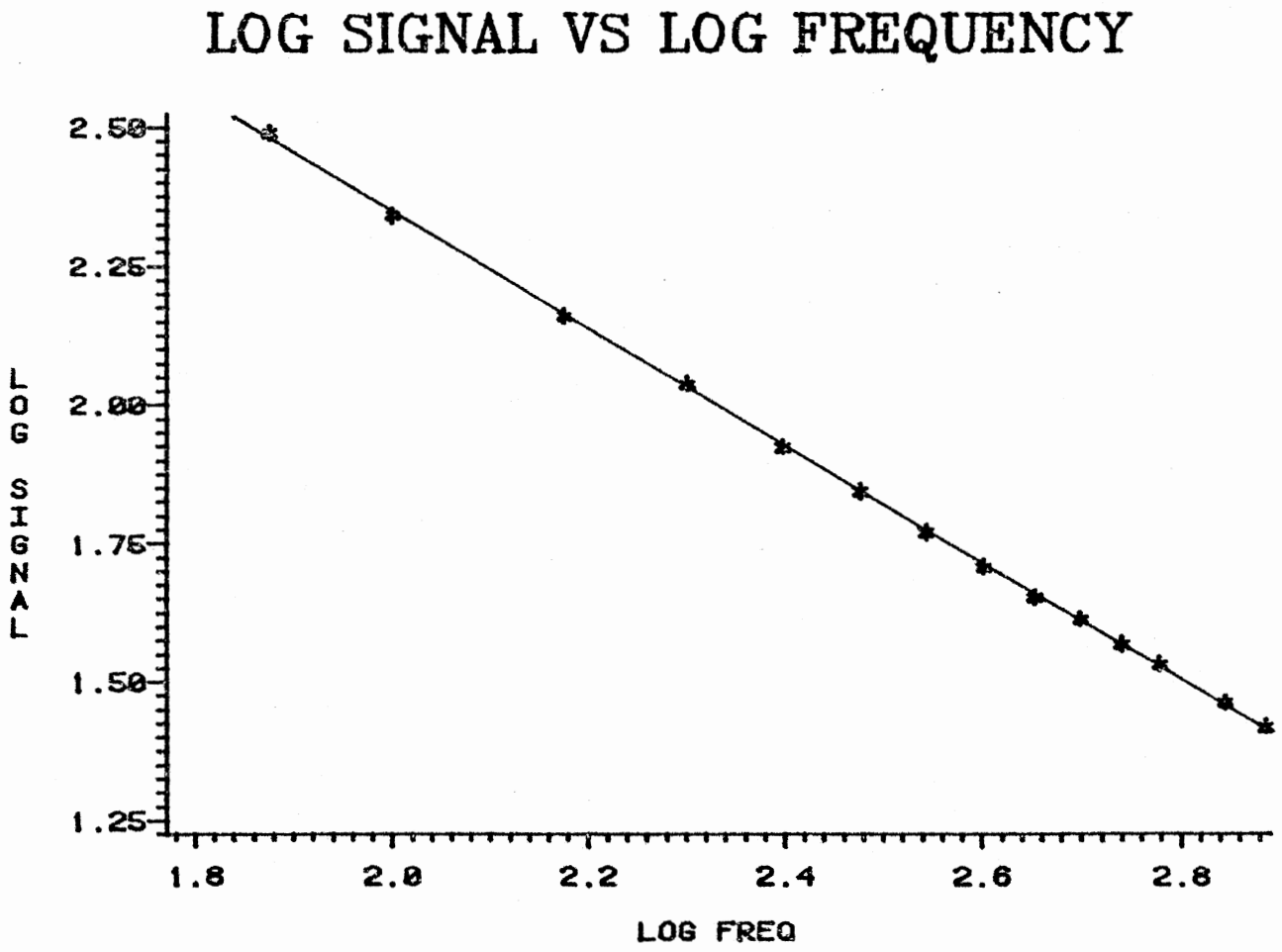

Figure 11. Plot of Log Signal vs. Log Frequency for the Right-Hand-Cell of the Differential Amplifier Arrangement. No Differential Amplifier is Used. The Slope is -1.047. The Sample is Carbon Black

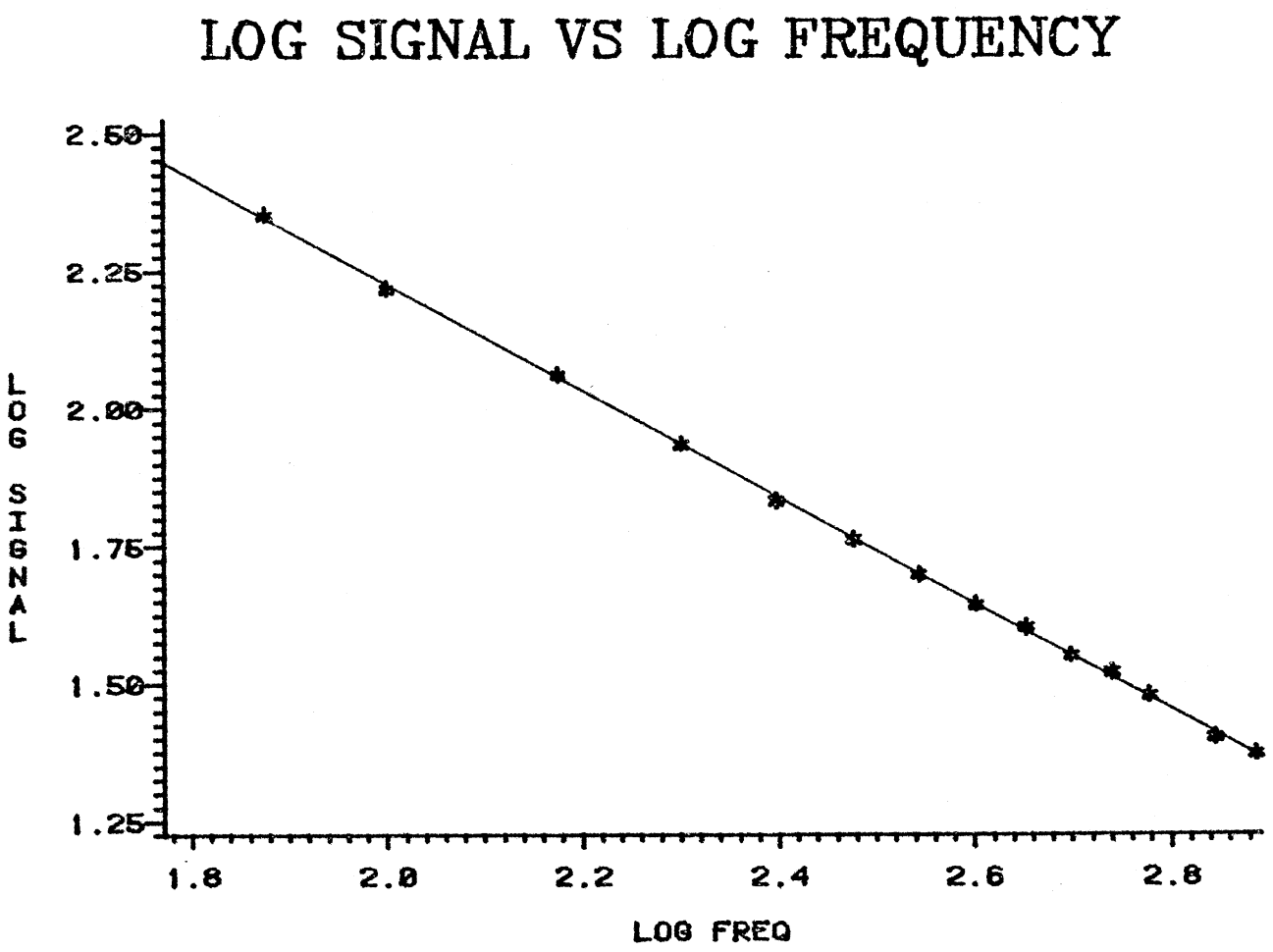

Figure 12. Plot of Log Signal vs. Log Frequency for the Replacement Cell. No Differential Amplifier is Used. The Slope is -0.970. The Sample is Carbon Black

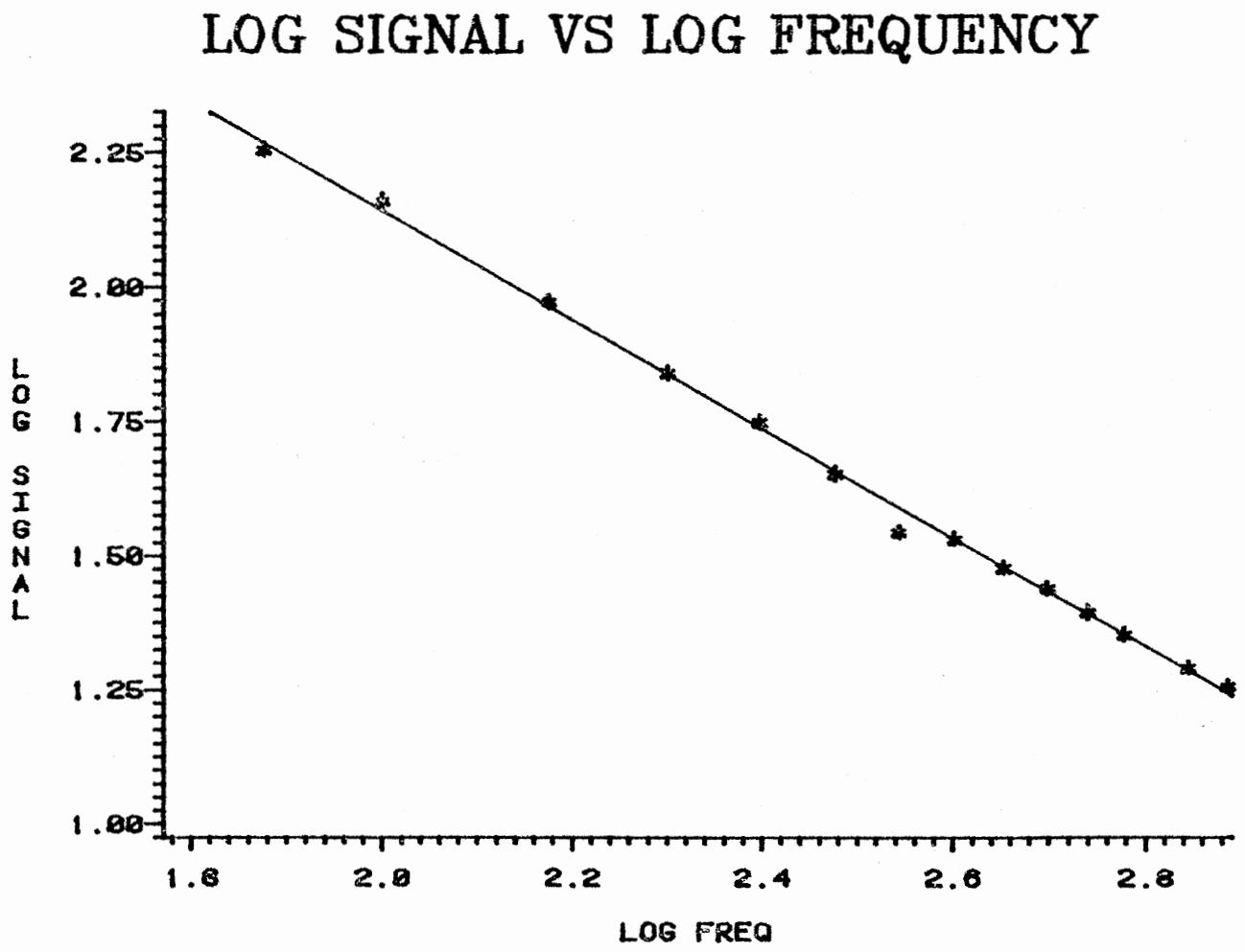

Figure 13. Plot of Log Signal vs. Log Frequency for the Right-Hand-Cell of the Differential Amplifier Arrangement. A Differential Amplifier is Used. The Slope is -1.032. The Sample is Carbon Black

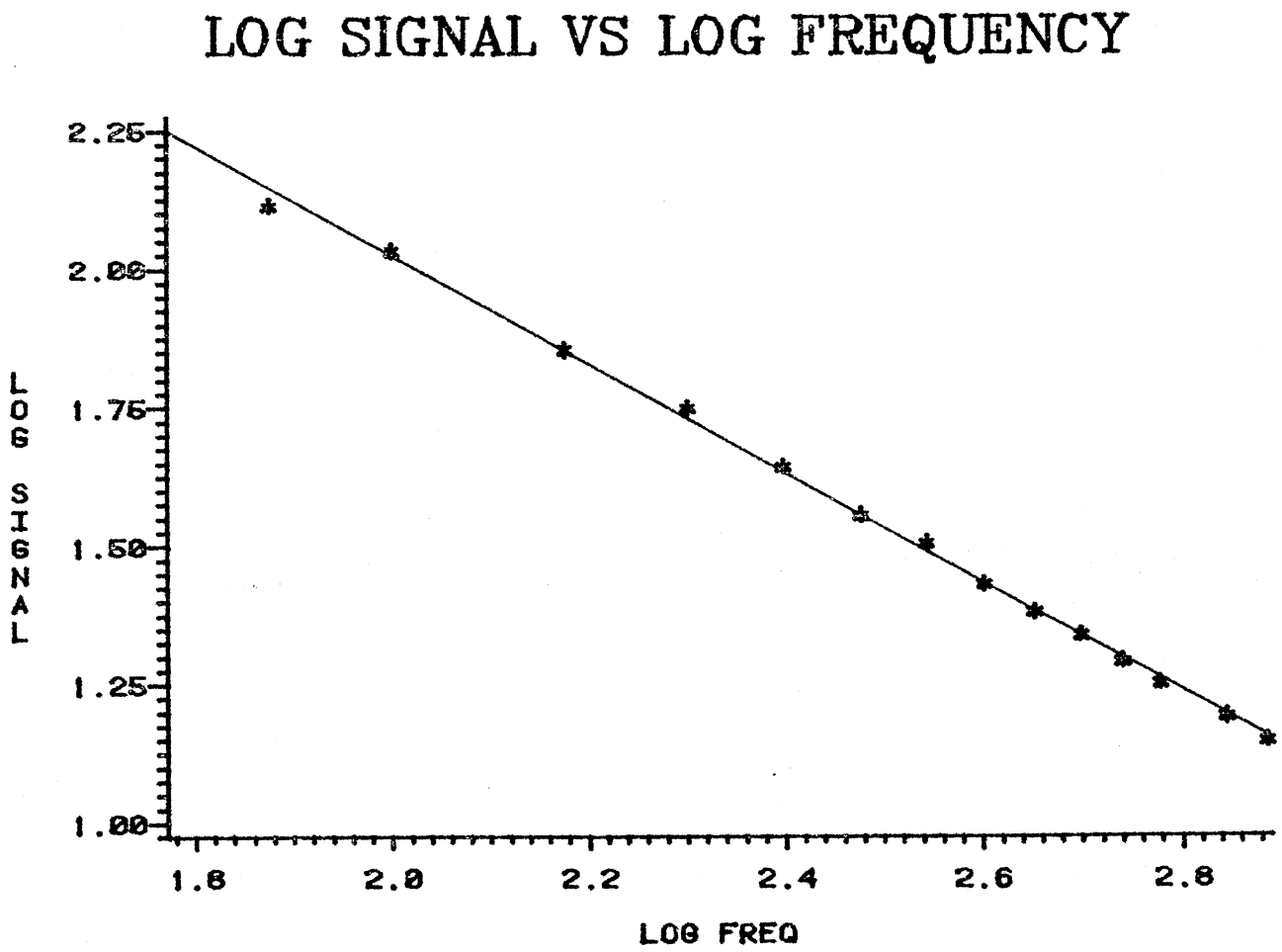

Figure 14. Plot of Log Signal vs. Log Frequency for the Left-Hand-Cell of the Differential Amplifier Arrangement. A Differential Amplifier is Used. The Slope is -1.003. The Sample is Carbon Black

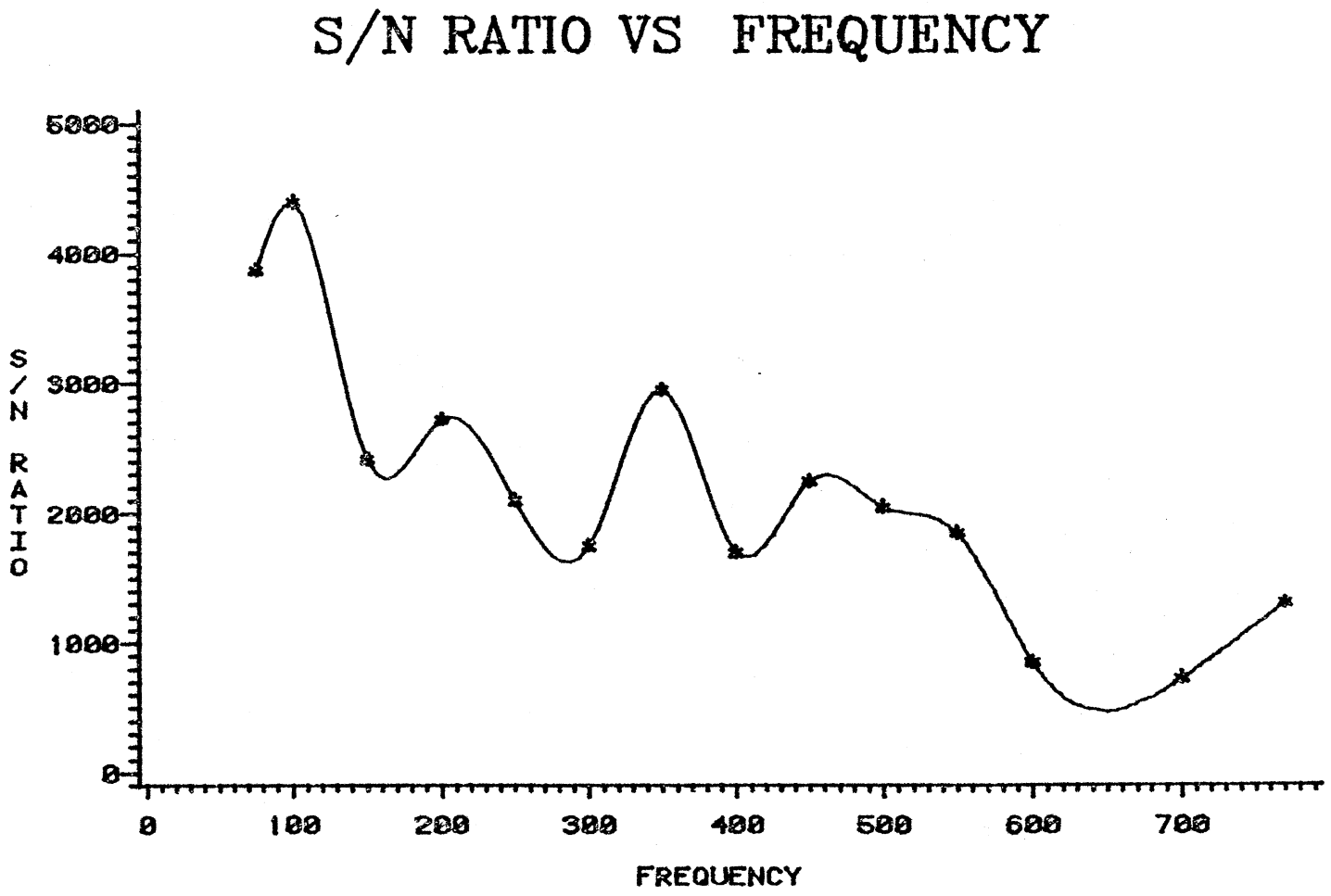

Figure 15. Plot of the Signal-to-Noise Ratio vs. Frequency for the Right-Hand-Cell of the Differential Amplifier Arrangement. The Sample is Carbon Black, and no Differential Amplifier is Used

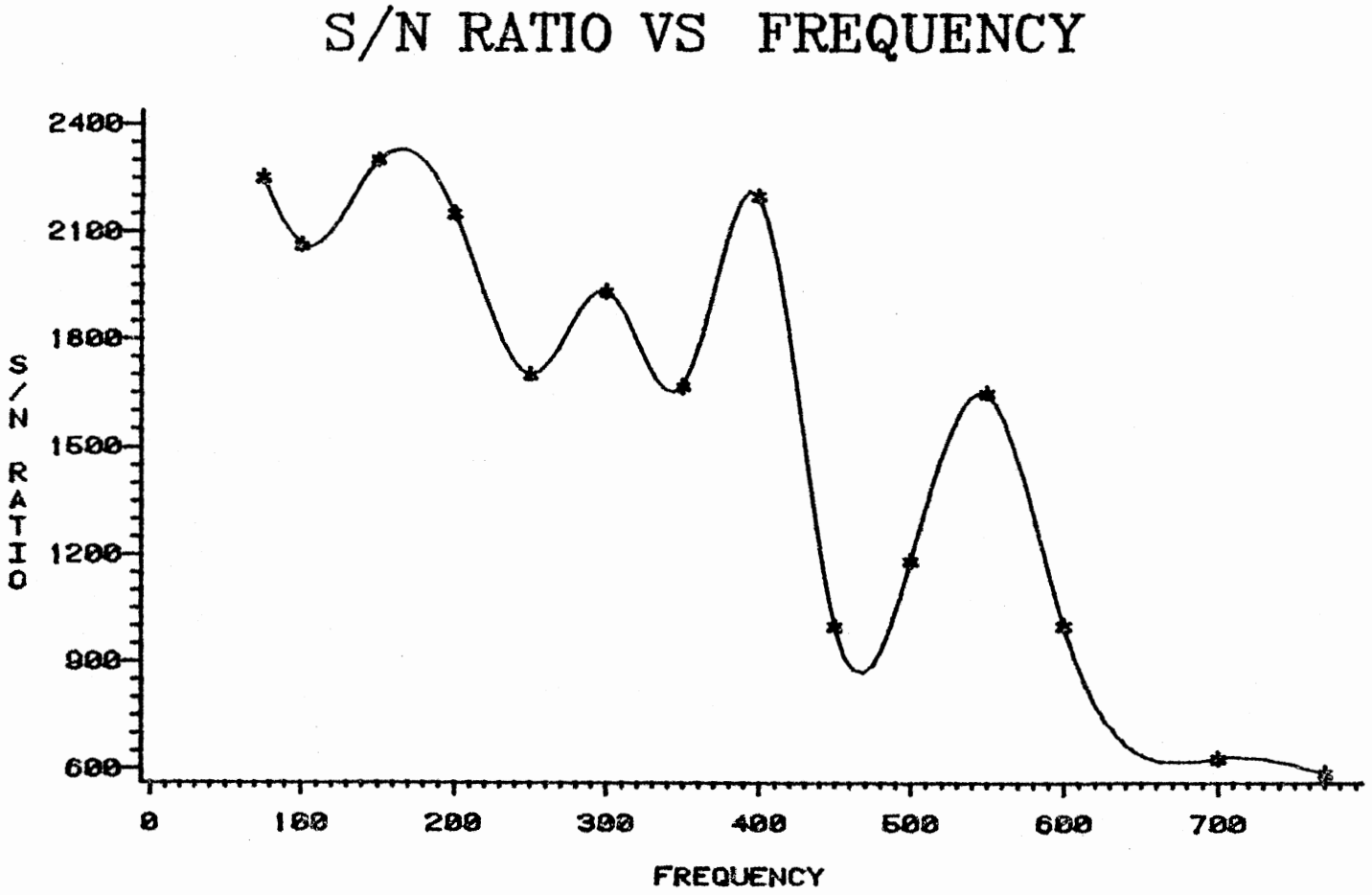

Figure 16. Plot of the Signal-to-Noise Ratio vs. Frequency for the Left-Hand-Cell of the Differential Amplifier Arrangement. The Sample is Carbon Black, and no Differential Amplifier is Used

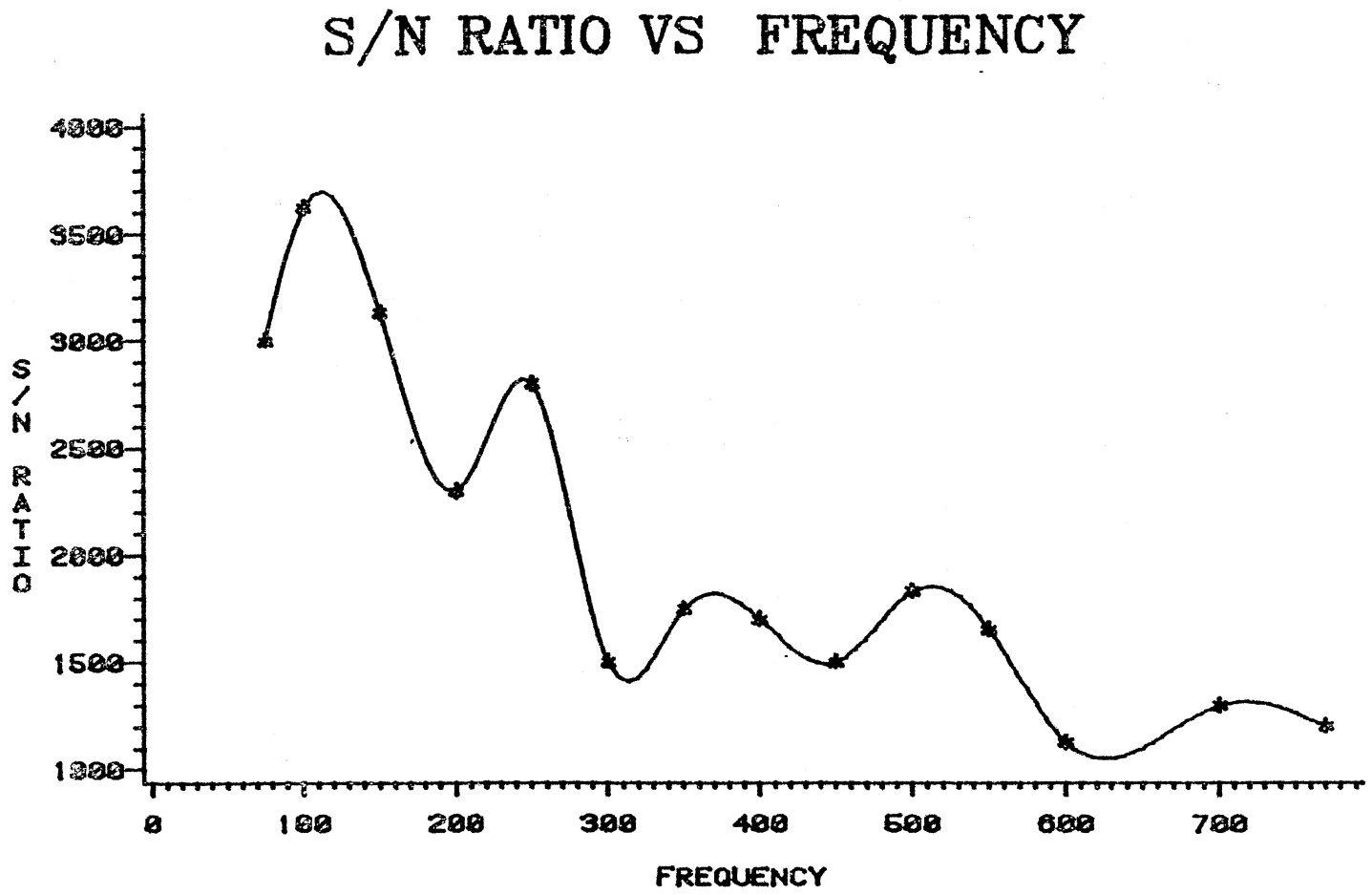

Figure 17. Plot of Signal-to-Noise Ratio vs. Frequency for the Left-Hand-Cell of the Differential Amplifier Arrangement. The Sample is Carbon Black, and a Differential Amplifier is Used

intensity of the signal (in millivolts) was divided by the peak-to-peak noise (in millivolts) and not the RMS noise.

Experimental Procedure

The experimental procedure which was used for the qualitative analysis of biological materials, the analysis of asbestos fiber, and the effects of particle size on the spectra remained constant. The first step in this procedure was to place hot molecular sieves in the bottom of photoacoustic cell, and cover these sieves with a small piece of aluminum foil. Next, the sample to be studied was placed in the cell, and the cell was sealed with a sodium chloride, NaCl, window. The cell was then placed in the spectrometer and the spectra taken.

The other samples, those used in the quantitative analysis of a binary mixture, the analysis of drug samples, and the analysis of amorphous carbon surfaces, required slightly more extensive preparations. The mixtures of the nitrate salts had to be weighed on a Mettler balance. These mixtures were weighed to within 0.0001 grams. The samples were than crushed in a Wig-L-Bug for approximately 2 minutes. The sample was then treated by the procedure mentioned above.

The analysis of drug samples was performed on samples prepared by John Bowen. These samples were prepared by Mr. Bowen to ensure that the quantitative analysis was carried out with as little experimental bias as possible. Once the samples were obtained, they were crushed in a Wig-L-Bug for approximately two minutes. The samples were then prepared as described above.

The most involved procedure is the one used for investigating the amorphous carbon surfaces. The procedure is as follows:

1. Wash lampblack with triply distilled water to remove water soluble ash,

2. Dry the lampblack in an oven at 200°C for 24 hours to remove the interstitial water, and

3. Allow the lampblack to cool in a vacuum desiccator until the lampblack is to be used. (A vacuum was pulled on the desiccator for about 2-2½ hours).

This preparation is also followed when dealing with charcoal rather than lampblack. The dried lampblack spectrum is then obtained by using the standard photoacoustic technique.

The various liquids or solutions used for studying the adsorption of various materials on lampblack were mixed with the dried lampblack. These mixtures were stirred together for a minimum of 24 hours, and the lampblack was then separated from the solution by filtration. This filtration was performed using a Whatman Number 3 Filter Paper. The lampblack was then air dried to remove liquid water and the various spectra were recorded.

CHAPTER III

RESULTS AND CONCLUSIONS

Three main questions of interest emerge in studying the photoacoustic effect of solids in the infrared region using a Fourier Transform Spectrometer. Could this technique produce good qualitative results? Could this technique produce good quantitative results? What factors affect the quality of the photoacoustic signal obtained? Experiments were designed to answer these questions.

The first set of experiments were intended to address the question of qualitative results. For this, three different types of solid samples were chosen: 1) a variety of biological materials of interest in body metabolism, 2) asbestos fibers playing a part in contamination of air and water supplies, and 3) biologically active drugs.

Biological Materials

The Fourier Transformed Infrared Photoacoustic Spectrum (FTIR-PAS) of protoporphyrin IX dimethyl ester (Figure 18), hemin (Figure 19), hemoglobin (Figure 20) and horseradish peroxidase (Figure 21) were run to determine if this technique yielded qualitative information. The spectra are shown in Figures 18-21.

The spectrum of protoporphyrin IX dimethyl ester (Figure 18) is qualitatively identical to that reported by Boucher and Katz (41). The only quantitative difference is in the relative absorbance of the methyl

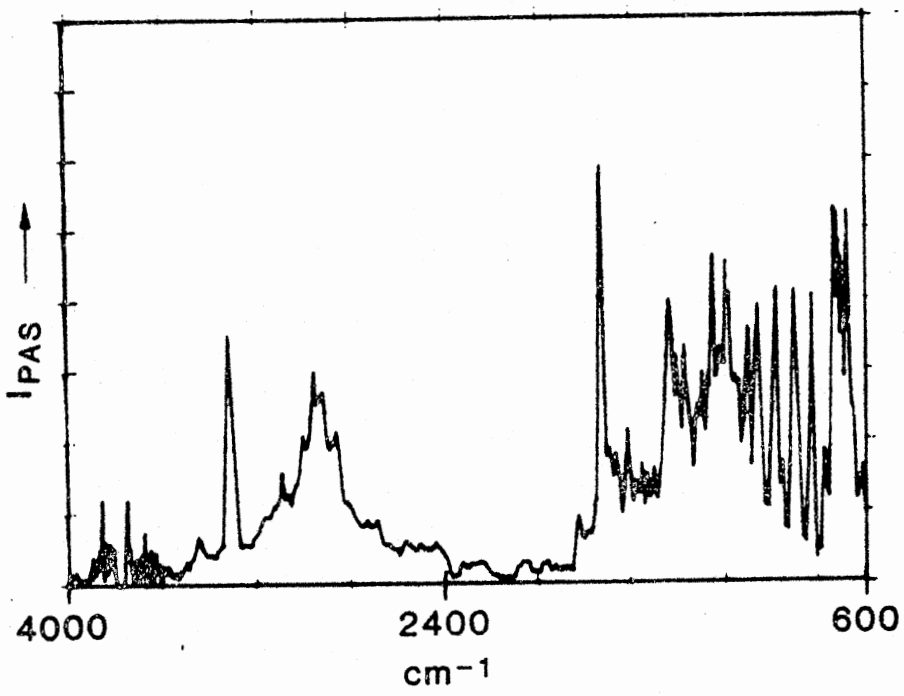

Figure 18. 800 Scans of 7 mg of Protoporphyrin IX Dimethyl Ester at 8 cm^{-1} Resolution. The Sample was Grade 1 Purity from Sigma Chemical Company.

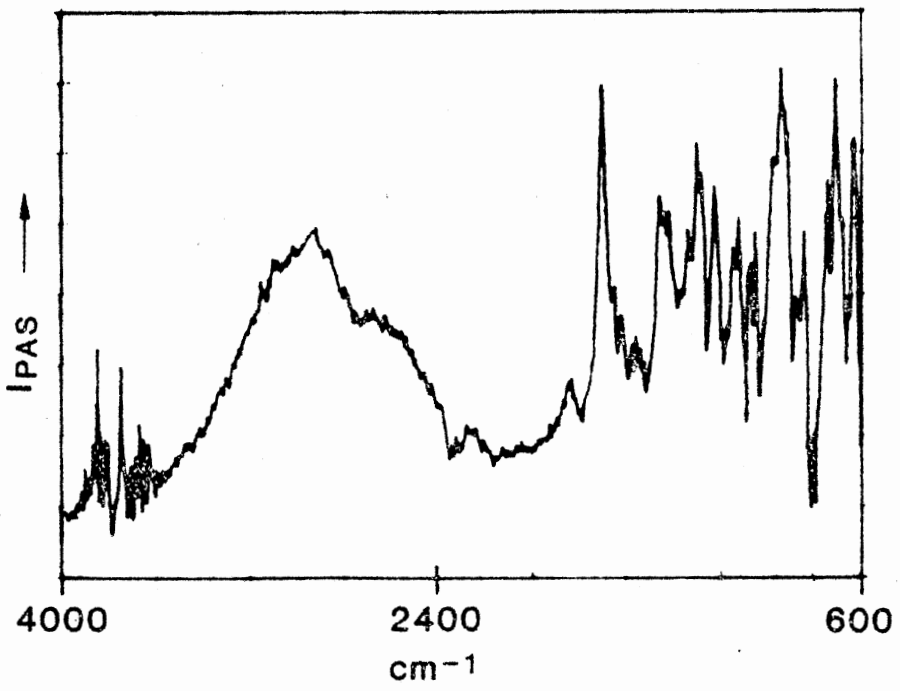

Figure 19. 800 Scans of 14 mg of Hemin-Bovine at 8 cm^{-1} Resolution. The Sample was Grade 1 Purity from Sigma Chemical Co.

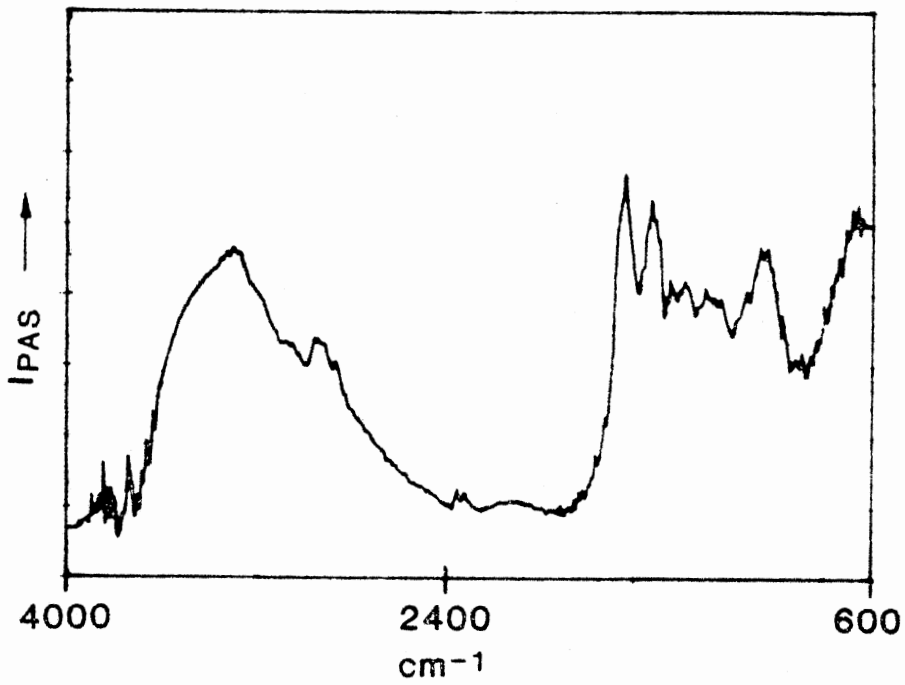

Figure 20. 800 Scans of 1 mg Hemoglobin at 8 cm^{-1} Resolution. The Sample is Hemoglobin from Beef Blood which was Obtained from Sigma Chemical Company.

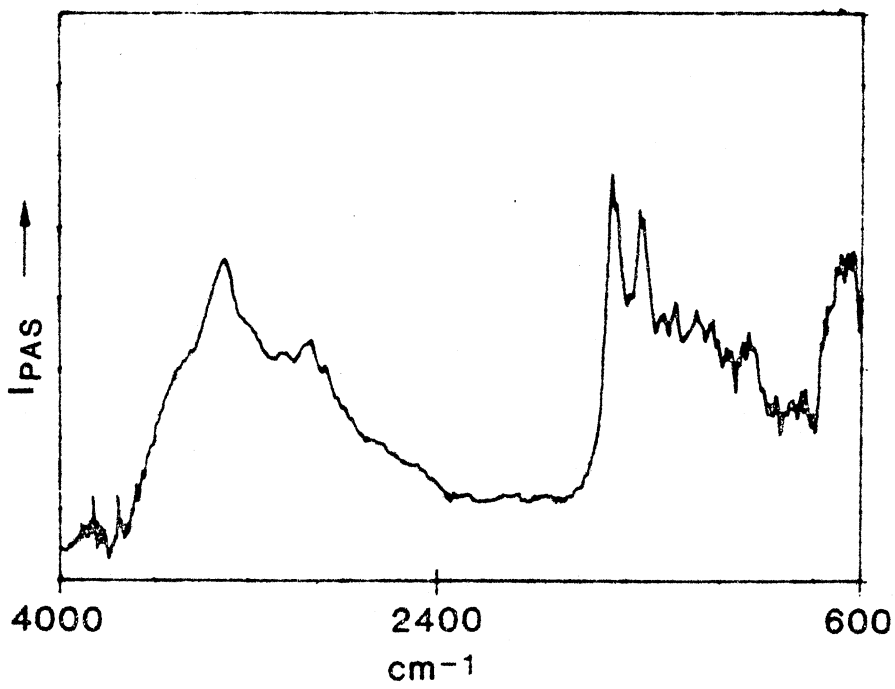

Figure 21. 200 Scans of 0.5 mg of Horseradish Peroxidase at 8 cm^{-1} Resolution. The Sample is Type VI RP Obtained from Sigma Chemical Company.

propionate ester carbonyl stretch at 1738 cm^{-1} seen by the two methods. By comparison with the rest of the spectrum, the PAS signal strength for this band is much less than that reported by Boucher and Katz. With this exception, the remarkable agreement between the spectra obtained by the two methods show that FTIR-PAS is capable of yielding structural information on undiluted solid samples without the need for samples preparation.

The spectrum of hemin (Figure 19) is remarkably similar to the conventional transmission spectrum (42). The sharp absorption due to the N-H stretch in protoporphyrin IX is absent in the spectrum of hemin, as expected. In hemin the nitrogens of the porphyrin ring structures are coordinately bonded to the iron in the center of the ring (Figure 22).

The spectra of hemoglobin, Figure 20, and horseradish peroxidase, Figure 21, are similar. They show broad, almost structureless, absorptions, again as might be expected. The wealth of different bonds found in the proteins attached to the central porphyrin structure crowd the spectra, with the result that little structural information can be inferred. Koenig and Tabb (43) performed a study on globular proteins in aqueous solutions. In their study several prominent bands were identified. These include the Amide I band at approximately 1660 cm^{-1}, the Amide II band at around 1540 cm^{-1}, and the Amide III band at 1245 cm^{-1}. The other prominent band in the hemoglobin spectrum, the band at around 1100 cm^{-1}, has been assigned to the γ_t of NH_2. Each of these bands are present in the spectrum of hemoglobin, Figure 20. The important fact here is that Koenig and Tabb (43) had to dissolve their samples in water, or prepare them as cast films, while the spectra shown in Figures 18 through 21 were run on pure samples with total weights

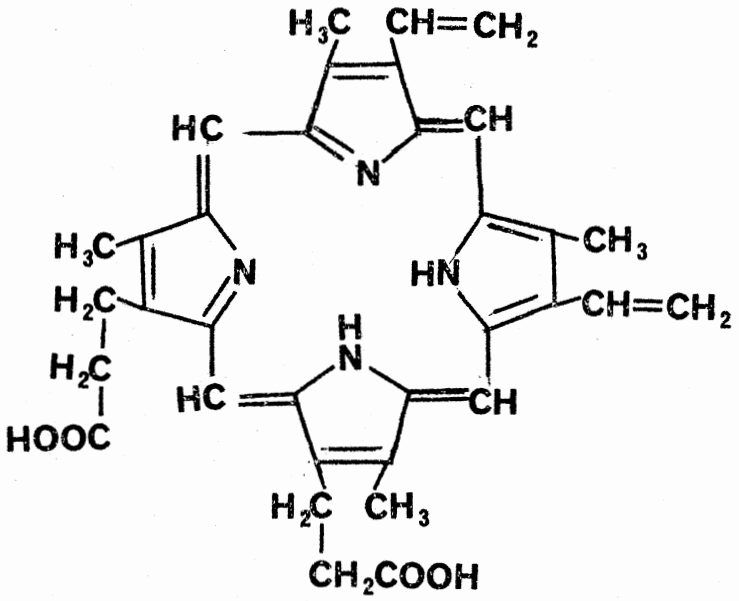

Figure 22. Protoporphyrin IX Dimethyl Ester.

of around 1 milligram each.

Asbestos Fiber

The prominence of asbestos fiber as a contaminant of water supplies has prompted the development of several detection schemes for measuring low concentrations of this fiber. One of the more ingenious schemes is that proposed recently by Monchalin et al. (44). Using a CW HF laser, this group was able to measure a few points (corresponding to the laser lines) on the photoacoustic absorption spectrum of asbestos fiber in the 3400 cm^{-1} to 3800 cm^{-1} region. They assigned the location for the two hydroxyl groups and showed that these absorptions were polarized. The suggestion was made that a photoacoustic detection scheme could be arranged using this anisotropic absorption as a distinguishing feature for the asbestos in the presence of other contaminants.

Because of this intriguing possibility, it was felt that a more detailed photoacoustic spectrum of asbestos fiber using the new technique of FTIR-PAS would be useful. The FTIR-PAS spectrum of asbestos fiber is shown in Figure 23. Several features of this spectrum are notable. Firstly, the sharp doublet at 3675 cm^{-1} due to the presence of non-hydrogen-bonded hydroxyls at two different locations within the crystallographic structure of asbestos (chrysotile) is apparent (44). The major peak has a maximum at 3692 ± 2 cm^{-1}, and the lesser peak is centered at about 3655 ± 5 cm^{-1}. These measurements are taken from an expansion of Figure 23 and agree, within experimental error, with those made by Monchalin et al.

Monchalin and coworkers (44) expected that the ratio of the intensities of the strongto weak bands in this doublet would be almost 3

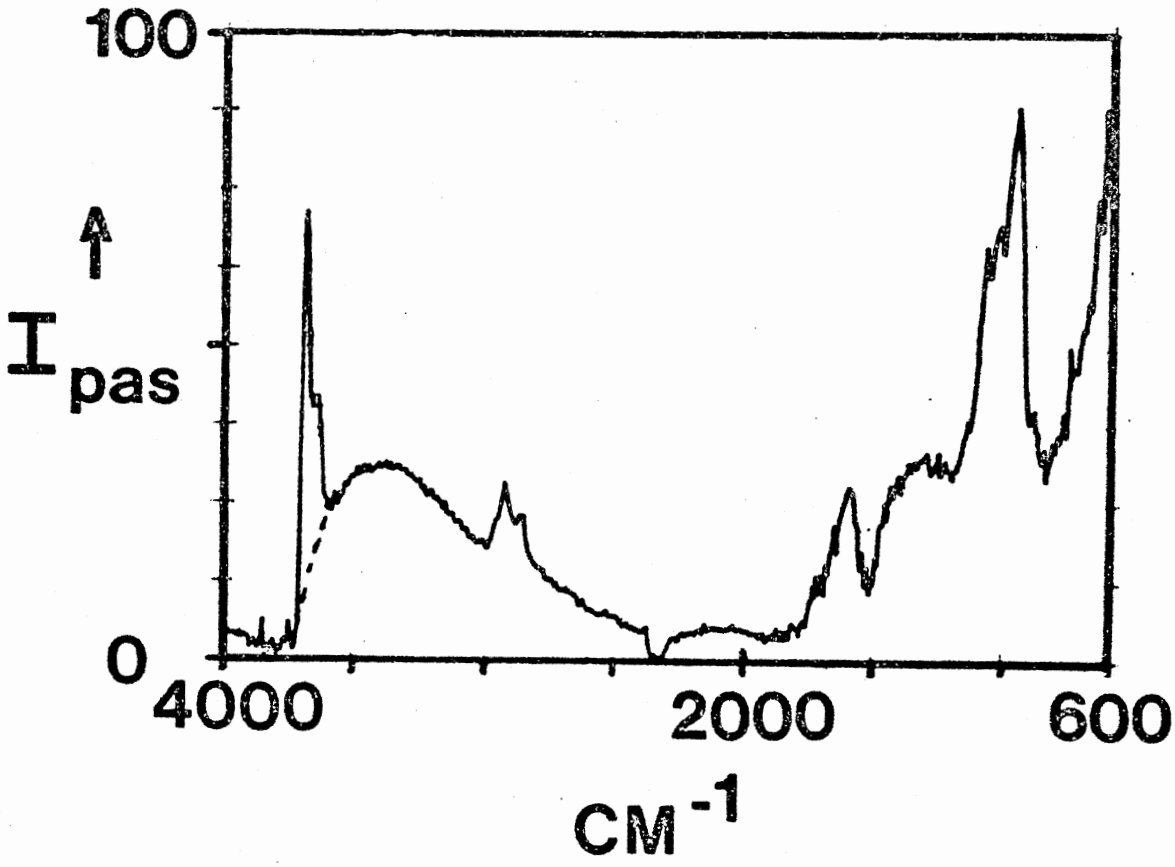

Figure 23. The corrected FTIR-PAS spectrum of asbestos fiber. 400 scans at 8 cm^{-1} resolution are coadded.

to 1, based on analysis of the crystallographic structure of chrysotile. However, because they were using a line source for excitation (an HF laser), they were unable to clearly define the maximum PAS signal of the two components of this doublet. It is tempting to extrapolate the absorption due to physisorbed water as has been done in Figure 23 (the dotted line) and then to obtain the net absorption strengths of the two components of the doublet (45). Analysis of an expanded spectrum in this manner does, indeed, yield a ratio of 3 to 1.

The final interesting feature of the spectrum in Figure 23 to be discussed here is the strong absorption at 945 cm^{-1}. It is readily apparent that this absorption is stronger than the absorption at 3692 cm^{-1} by about 25%. Coincidentally, the absorption is also centered at the emission wavelength of the CO_2 laser. Since the CO_2 laser is more convenient to use in any detection scheme than an HF laser, and since the chrysotile PAS absorption at the CO_2 laser wavelength is stronger than at the HF laser wavelength, the CO_2 laser may well be the preferable excitation source for detection of asbestos fibers by photoacoustic spectroscopic methods. In addition, the band at 945 cm^{-1} lies in the fingerprint region, which is unique, for this mineral class.

Quantitative Results

In the attempt to determine if the FTIR-PAS signal strength was correlated with the percent by weight concentration of the sample, the spectra of a set of mixtures of $K^{15}NO_3$ and $K^{14}NO_3$ were made. The $K^{15}NO_3$ was obtained from J.P. Devlin who purchased it from Stohler Isotope Chemical Company, while the $K^{14}NO_3$ was purchased from the Baker Chemical Company. Both chemicals were 99% isotopically pure. A set of mixtures

of the two salts were carefully weighed. They were then ground with an agate mortar and pestle to increase the sample surface area and to insure sample homogeneity. In practice, the FTIR-PAS signal strength is dependent upon the particulate size. However, because these experiments relied on the measurement of relative absorption peak heights of the two salts, (Table I, Appendix), the absolute signal magnitude was not an important consideration, provided the samples were homogeneous. Consequently, the salt mixtures were not sized.

Figure 24 shows the unsmoothed, unretouched FTIR-PAS spectra of pure KNO_3 and a mixture of the two KNO_3 salts. While the compressed spectra look quite similar, the inset, which shows an expansion of the spectrum in the vicinity of the γ_2 absorption at 825 cm^{-1}, clearly shows the isotopic shift expected and the presence of the two components in the 50:50 mixture. The bottom spectra are of the pure $K^{14}NO_3$, while the top are spectra of a 50:50 mixture of $K^{15}NO_3$ and $K^{14}NO_3$. One other notable feature shown in the insert of Figure 24 concerns the relative peak heights apparent for the 50:50 mixture. The absorption band centered at 825 cm^{-1} for the ^{14}N salt tails off to about 20% of the maximum intensity at 800 cm^{-1} where the γ_2 absorption of the ^{15}N salt appears. Thus, the ^{15}N absorption appears to be more intense in the 50:50 mixture, but only by virtue of being situated on the shoulder of the ^{14}N.

A peak resolving routine would have made the analysis of these samples easier and more accurate, as the two peaks are not perfectly separable. The peak resolving routine would separate the two peaks into their relative contributions, thus making the measurements trivial.

To obtain an estimate of the quantitative dependence of the FTIR-PAS signal strength on the relative percentage of each salt, the γ_2

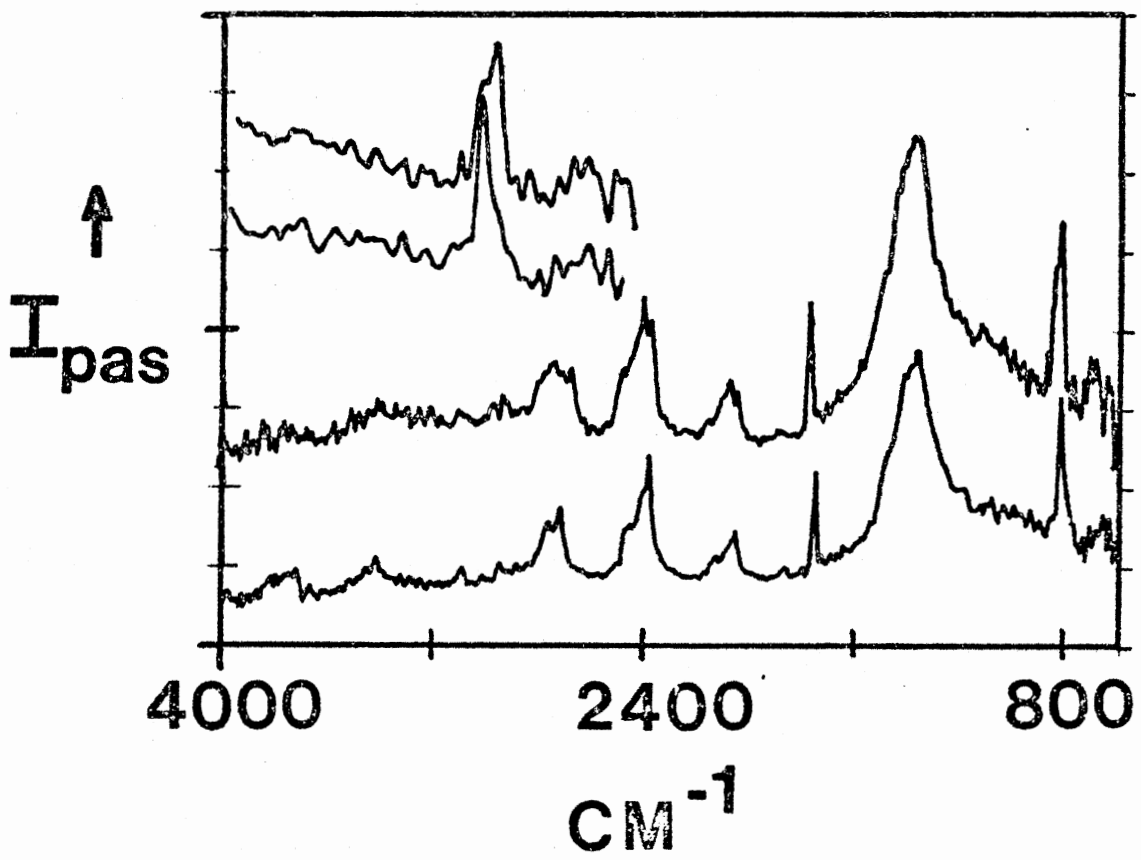

Figure 24. The ETIR-PAS spectra of $K^{14}NO_3$ (lower spectrum) and $K^{15}NO_3$ (upper spectrum). The inset shows an enlargement of the two spectra in the vicinity of the 825 cm^{-1} absorption. 1000 scans at 8 cm^{-1} resolution were coadded for each spectrum.

absorption feature at 825 cm^{-1} was analyzed vs. the intensity of this absorption feature (generally consisting of two bands, due to the two different salts) at 800 cm^{-1} and 825 cm^{-1}. In this manner, a relative signal strength for the ^{15}N salt absorption was obtained for each mixture. The reliability of this approach was verified by measuring the FTIR-PAS spectra of the pure salts individually, adding the two spectra together in different percentages and analyzing this synthetic data in the same fashion as described above (Table II, Appendix).

Figure 25 is a graphical representation of the relative absorbance by $K^{15}NO_3$ as a function of the weight percentage of the salt in the mixture. A least squares fit of the data gives a straight line with a slope of .65 and a correlation coefficient of .98. This line intercepts the ordinate at .24. This is not to say that $K^{15}NO_3$ was 25% $K^{15}NO_3$. Rather this intercept represents the relative height of the shoulder on the $K^{14}NO_3$ absorbance. For similar reasons, 100% $K^{15}NO_3$ registers as 90% purity. That is, there is a smaller but finite high frequency tailing of the $K^{15}NO_3$ absorption.

Particle Size

One parameter affecting the quality of spectra is the effect of particle size of the sample upon peak height. The first theoretical treatment of this subject is attributed to Lord Rayleigh (46) who concluded that the amount of scattering was inversely proportional to the fourth power of the incident wavelength, and is directly proportional to the cube of the particle diameter size. Lower scattering at lower frequencies and lower particle sizes would be expected. This has been noted in the study of surface hydroxyls in which the quality of the

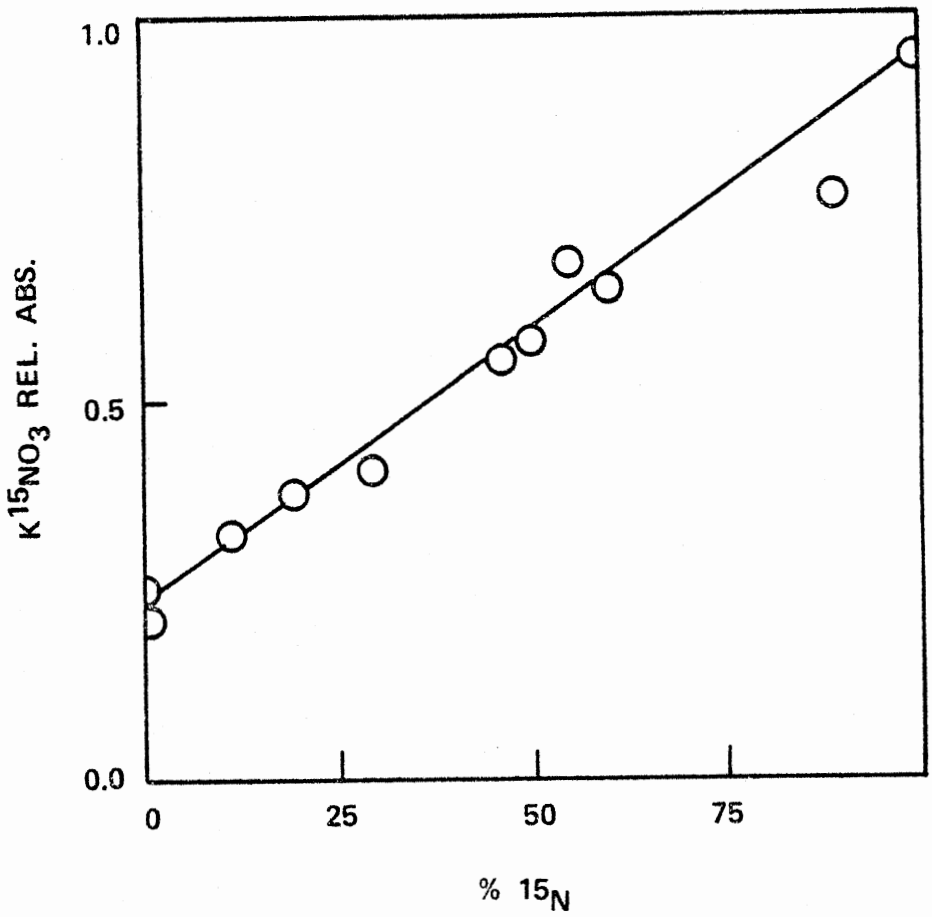

Figure 25. Relative Peak Intensity at 800 cm^{-1} vs. 825 cm^{-1} Plotted Against $\%K^{15}NO_3$. The Least Squares Line Fits the Data with a Correlation Coefficient of 0.98

spectrum obtainable with deuterated samples was superior to the quality of the hydrogenated samples (47). The OD peak is around 2700 cm^{-1}, while the DH peak is around 3600 cm^{-1}. Since the OD peak is at lower frequencies, the signal intensity would be expected to be greater, because the scattering would be less.

A study of the amount of scattering produced by a collection of particles was made by Duyckaerts (48). He assumed that particles of density "p " and diameter "d" were dispersed randomly in a disk of cross sectional area "S", mass "M" and length "l". He also assumed that the disk was arranged in "N" layers, and that the incident light interacts with each particle only one time. He concluded that

$$I / I_0 = (1 - K) + K \theta^{N} \tag{33}$$

where "K" represents the geometrical fraction of the surface where the light is focused, and θ is the transmission of one particle. From Beer's law the following equation is obtained.

$$\theta = \exp (-\alpha d) \tag{34}$$

α is the true extinction coefficient of the material. From the above equation the following equation is obtained.

$$\log I_0 / I = A = -N \log (1 - K) + K\theta \tag{35}$$

Determining "N" from p, d, S, M, K, Duyckaerts obtained

$$A_{\lim \alpha d \to o} = M \alpha / Sp2.3 \tag{36}$$

He plotted 2.3 A S p/M against d and showed that the maximum transmission was obtained when the particle size was less than the wavelength of the incident light.

To obtain an estimate of the importance of this phenomena in FTIR-PAS measurements, a study centered on AC fine test dust, from General Motors which was hydrodynamically separated in an air flow current, of

known particle sizes. The samples were 0-5 microns and 55-60 microns (Figure 26), 10-15 microns, 20-25 microns, 30-35 microns and 50-60 microns (Figure 27). The peak of interest was the peak around 1100 cm^{-1}, which is due to the Si-O stretch. A comparison of different particle sizes with respect to photoacoustic spectroscopy was expected to confirm Duyckaerts' findings. The peak height was analyzed in the usual fashion of relative peak intensity. For example (Table III, Appendix), the peak height for the 0-5 micron silica dust was found to be 74. The baseline signal at around 2500 cm^{-1} was 14. Therefore, the relative peak height of the signal at 1100 cm^{-1} is (74-14)/14, or 4.29. The reason for using this relative scale is to eliminate any differences from samples due to misalignment of the cell. The particle size that is associated with wavelength of light at 1000 cm^{-1} is approximately 10 microns. As the particle sizes approached this wavelength from larger particles, the band intensity relative to the background was enhanced considerably (Figure 28). Thus, the same effects for transmission spectroscopy and DRIFT (49) with respect to solid particle size applies to photoacoustic spectroscopy as well. Since Duyckaerts concluded that the resolution should also be affected by particle size, more work needs to be done to determine if this holds for photoacoustic spectroscopy as well. An assumption used by Duyckaerts was that the particles were embedded in a medium of equal refraction index. Since this is clearly not the case in gas-solid interfaces, more work also needs to be done to determine the relationship between signal enhancement and the difference between the refractive indices of the solid and gas interface.

The photoacoustic effect has been shown to depend upon the modulation frequency utilized. Therefore, care must be taken with sample

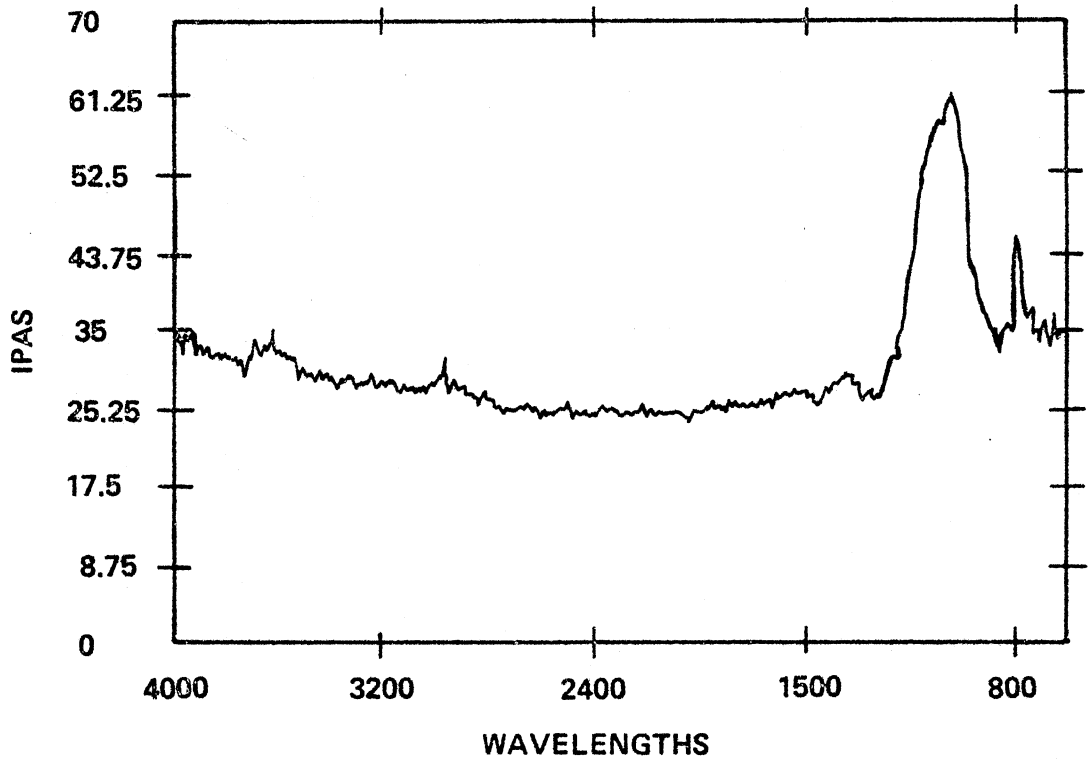

Figure 26. 1000 Scans of Silica Dust at 8 cm^{-1} Resolution. The Particle Size is 0-5 Microns

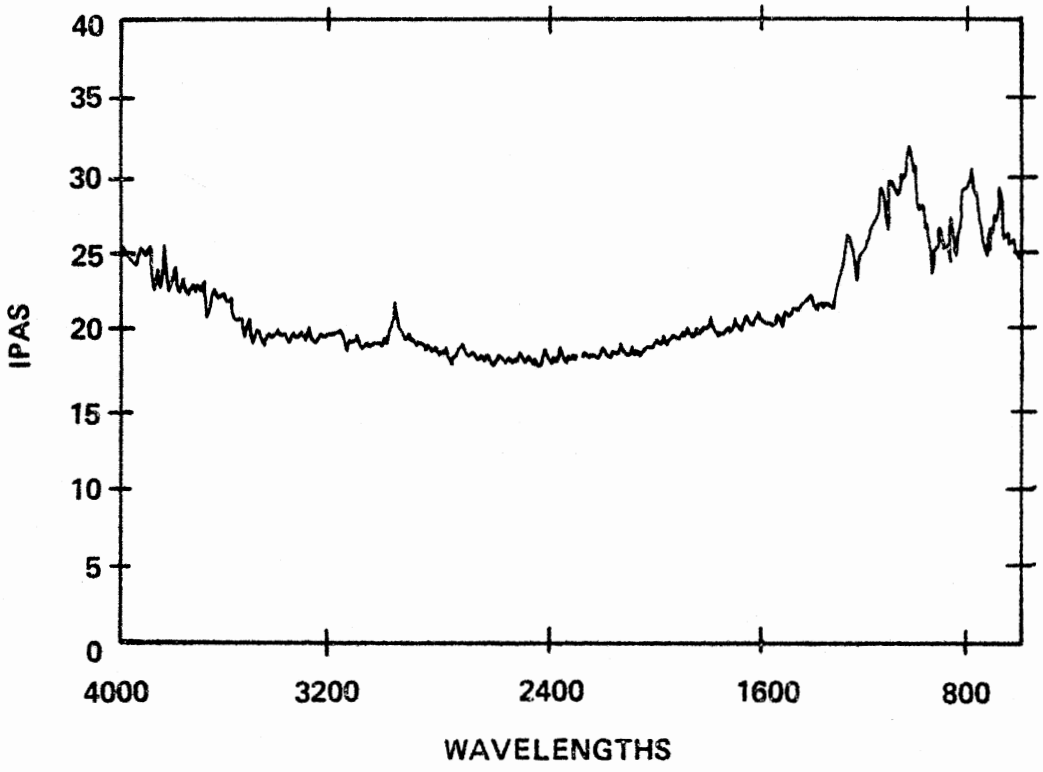

Figure 27. 1000 Scans of Silica Dust at 8 cm^{-1} Resolution. The Particle Size is 55-60 Microns

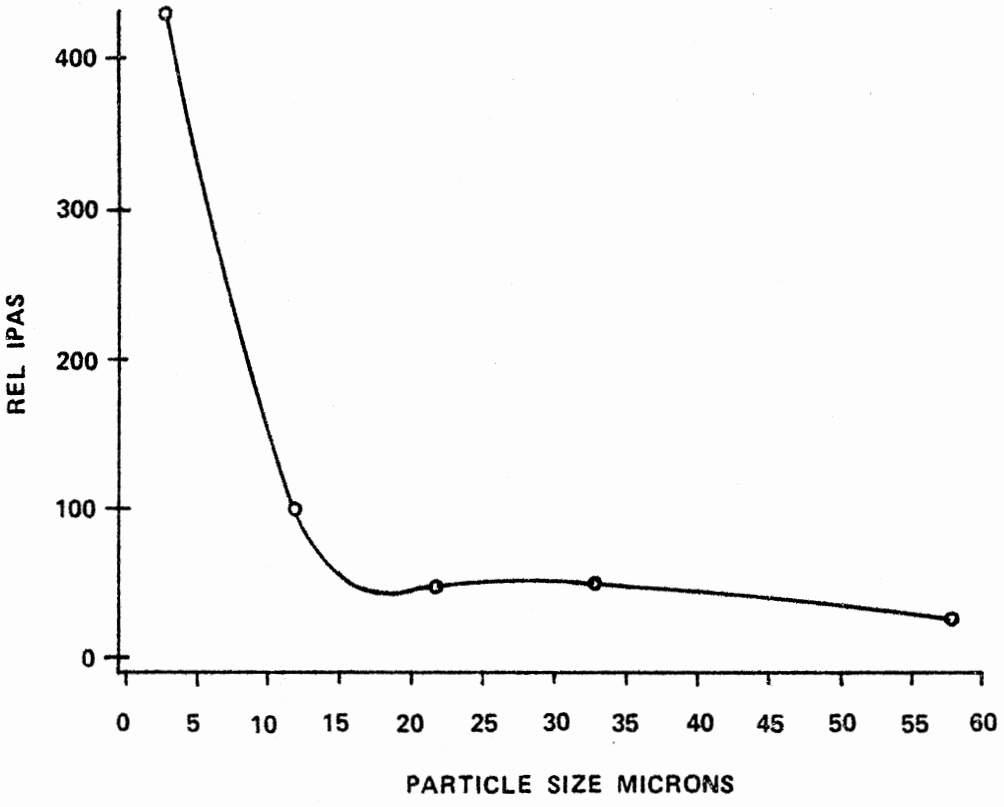

Figure 28. Plot of Relative I_{PAS} vs. Particle Size of Silica Dust in Microns, at 1000 cm^{-1}

preparation. Because the FTIR-PAS spectrum arises from sampling depths which vary with the infrared modulation frequency, the previous samples were considered homogenous. If, however, the media were not homogeneous, this factor must be taken into account. Certain external parameters were shown to play an important role in determining the quality of spectra obtainable. The cell design as well as the microphone used were closely linked to the number of scans necessary to obtain enhanced signal-to-noise ratios. The particle size of the condensed media was also shown to affect the signal intensity of the photoacoustic effect. The enhancement of signal at lower frequencies is believed to be due to an increased scattering of the sample. However, experiments have not been conducted to determine how the resolution of the FTIR-PAS spectrum is changed by particle size and the dependence upon the refractive index of the media used.

Forensic Analysis

Every conceivable analytical technique has been applied to the difficult problem of drug analysis (50). Because drugs are minor constituents in rather complex mixtures, a primary requirement in almost every analysis is to first effectively separate the mixture and, in so doing, concentrate the drug so that it has a concentration which exceeds the limits of detection of the method to be used. Qualitative identification is readily accomplished by the many chromatographic procedures either alone or in tandem with mass spectrometry or, in some cases, by spot tests. Quantitation is less readily accomplished and frequently requires compound derivatization and repeated instrument calibration.

Innovative techniques which can simplify the analytical protocol

either by requiring less stringent separation needs or by eliminating subsequent sample pre-preparation steps are valuable in that time, a precious commodity in clinical and criminalistic laboratories, is saved. A recent innovation, for example, is the application of circular dichroism spectropolarimetry (51) to the direct analysis of drugs.

A rapidly emerging technique which has the potential to expedite analysis is photoacoustic spectroscopy (PAS) (20,52). Its use in the ultraviolet spectral range was described in the early literature and, more recently, reports have appeared for the application of PAS in the mid-infrared range by both dispersive (28,30,53,54) and Fourier-transformed methods (FTIR-PAS) (35,37,39,55). The advantages of FTIR-PAS over dispersive methods are well delineated in these articles. They include speed of analysis, high incident power (useful for PAS studies) and frequency multiplexing. The disadvantages of FTIR-PAS are that the sampling depth varies with frequency, there is some difficulty in knowing exactly what to use as a power correcting reference spectrum and the thermal and optical properties of the samples control the frequency dependence of the PAS signal strength. These difficulties have been discussed in some detail by Krishnan (56) and by Royce et al. (57). These disadvantages notwithstanding, it was felt that for routine quantitative and qualitative analysis the currently used methods of FTIR-PAS analysis would prove to be a significantly useful tool in the modern forensic analysis laboratory by virtue of the speed of analysis, use of commercially available components, and other features described below.

This section describes the direct quantitative determination phenobarbital and phencyclidine (PCP) using FTIR-PAS. Sample mixtures, in powdered solid form, were all in-house preparations and were tested

for both the qualitative and quantitative capabilities of the method. The samples were prepared gravimetrically and made somewhat homogeneous in composition by shaking for 5 minutes in a Wiggle-bug. Reference FTIR-PAS spectra of the pure components of the various mixtures were stored on disk for subsequent subtraction as will be explained below.

PCP was phencyclidine hydrochloride obtained from NIDA via Research Triangle Institute. Parsley was from a local grocery store. This mixture was coground. Phenobarbital was from Sigma. Lactose was from Aldrich.

Two component mixtures were made with the compositions of these mixtures being made known to the individual running the FTIR-PAS spectra. In this way a so-called calibration line was inferred. The calibration line was prepared by substracting the spectra of the individual pure components from the spectra of the mixture and repeating the process until the flattest possible baseline was obtained, as shown by Figure 29 for the case of 12.1% by weight phenobarbital in lactose.

Following the experimental derivation of a calibration line or curve (for all cases studied here the set of points was well correlated with a straight line) a few samples ("blinds") were analyzed in which the concentration was known to the preparer but not to the analyst. Those points are represented by the asterisks in Figure 30.

Results and Discussion

An illustration of some typical spectra is given in Figure 29 for the case of a 12% by weight phenobarbital in lactose system. The top spectrum is that of the mixture phenobarbital in lactose system and the bottom spectrum is that which remains after 0.12x the pure

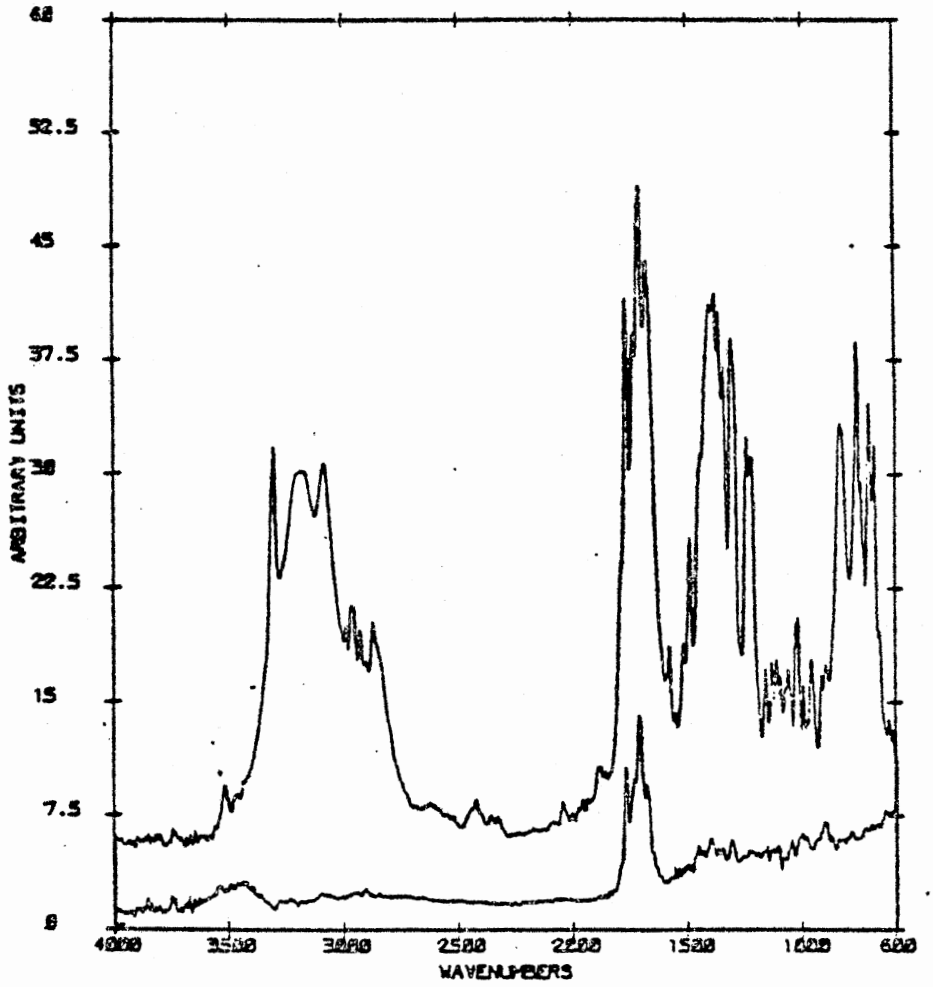

Figure 29. Top Spectrum is that of Ca. 10 mg of Pure Phenobarbital with 2000 Scans at 8 cm^{-1} Resolution, Corrected by Reference to a Carbon Black Spectrum. Bottom Spectrum is the Residual Spectrum from 2000 Scans at 8 cm^{-1} Resolution of 12.1% by Weight Phenobarbital in Lactose after Subtracting the Spectra of the Pure Components in a 0.12 to 0.88 Ratio of Phenobarbital to Lactose.

lactose spectrum and 0.88x the pure phonobarbital spectrum are subtracted from the spectrum of the mixture. It can be seen that the baseline is essentially flat with the notable exception of the band at ca. 1700 cm^{-1}. The flatness of this baseline was estimated by eye and was not further analyzed by any computer algorithm, although with the purchase of suitable software this could also have been done. After several trials it was determined that the band at 1700 cm^{-1} which remains outstanding after spectral subtraction of the component spectra is not quantitatively related to the amount of phenobarbital in the mixture. While the exact cause of this outstanding feature has not been determined here, it is hypothesized that it could be due to a number of different phenomena. It could be that the pure component spectrum of phenobarbital was measured with a sample which had a slightly different grain size distribution than that present in the mixtures. In such a case, the amount of reflected light might be different at that particular band. That is, the phenomenon would correspond to some sensitivity of the photoacoustic spectrum to the amount of reflected light, especially for the case of intense transitions where the amount of scattered or reflected light will be greatest. Another possible cause for this phenomenon which also could be explained on the basis of variations in the distribution of grain sizes is the occurrence of saturation (56,58). Since the presence of saturation in the generation of the photoacoustic signal is dependent on the ratio of the thermal to the optical thickness of the sample, the appearance of this anomaly in band intensity could be associated with differing amounts of signal saturation present in the pure and mixed samples for absorption into this particular band. As to whether or not either of these two reasons is correct requires the

analysis of a series of samples in which the grain size distribution of the pure and mixed samples are tightly specified. Even then it is not clear that the relative surface areas for the two samples would be the same. Nevertheless, it might be that the amplitude of this anomalous feature would decrease with decreasing grain size in which case at least one of these two proposed origins might apply. Finally, it is possible that Kubelka-Munk corrections, which are necessary to correct band intensities for reflectivity variations, might prove useful in distinguishing saturation from reflection problems.

Despite these difficulties, the relative compositions of the various mixtures were obtained by spectral subtraction procedures. Adequate subtraction was inferred by assessing the flatness of the subtracted spectral baseline in regions outside of those containing intense features. Table IV contains the results obtained for the analysis of phenobarbital and lactose. To show the linearity of the measured vs. given weight percentages, the data in Table IV are plotted in Figure 30. In all cases the percentages are accurate to within 1% and have a precision of better than 1% as shown by multiple but independent analyses of the same unknowns. For the two measurements of the same unknown, two independent samples were obtained from the container of sample provided.

The PCP on parsley system was analyzed in similar fashion and the data are described in Table V. The accuracy of the measured results here is not quite as good as for the case of phenobarbital and lactose. That is to be expected, however, since the samples of PCP on parsley cannot be made nearly as homogeneous as the phenobarbital and lactose system.

As a result, sampling errors become more significant. The

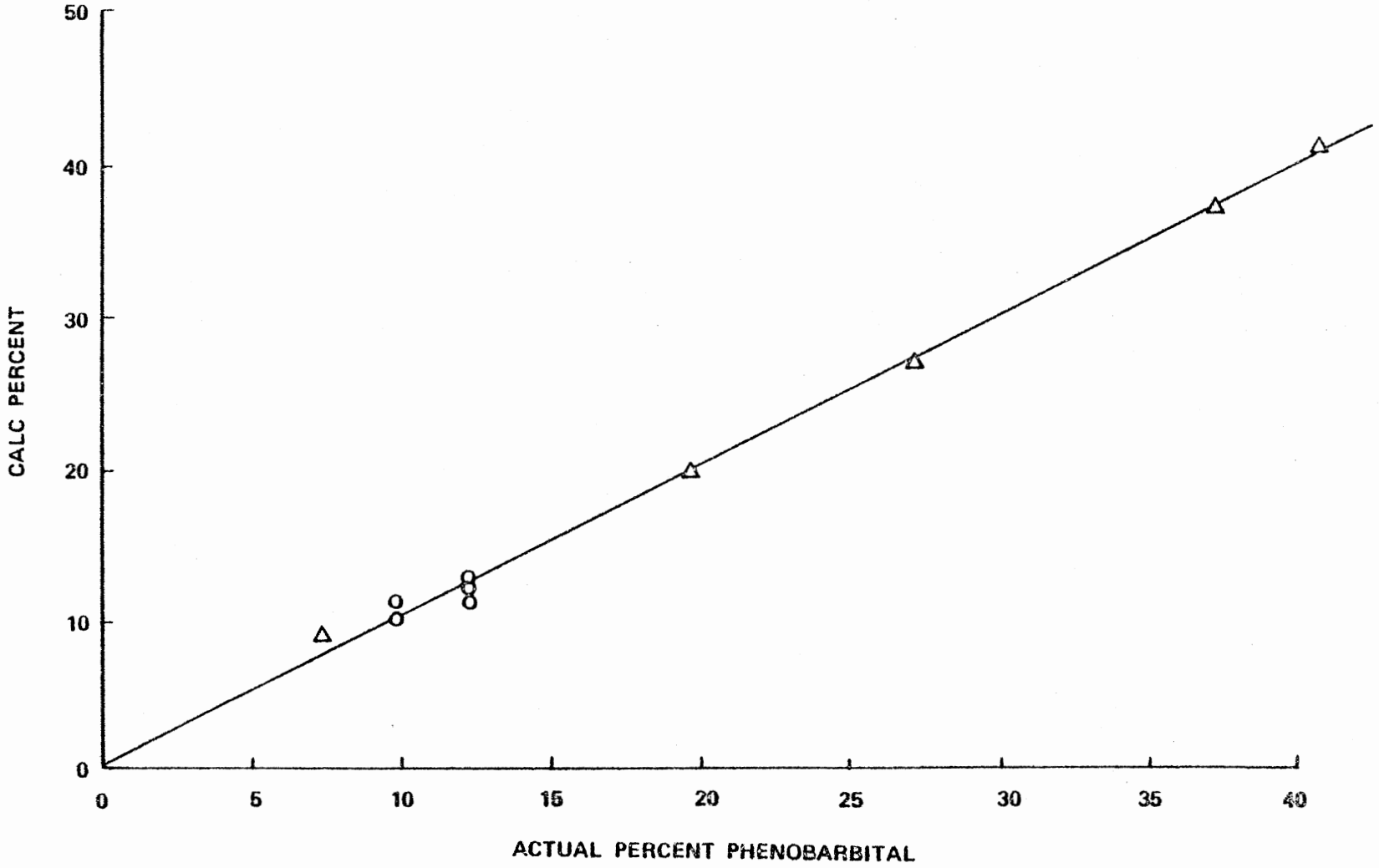

Figure 30. Plot of calculated or measured weight percent phenobarbital in lactose (by FTIR–PAS) vs. gravimetrically defined weight percent. O represents unknowns while △ represents knowns.

presence of two strong bands centered at 1600 cm^{-1} and 1100 cm^{-1} in the spectrum of parsley could not be subtracted totally from the spectra of the mixtures, indicating the presence of the saturation and reflectivity problems also apparent in the phenobarbital-lactose system. The parsley was also incompletely dried. This resulted in the introduction of significant quantities of water vapor into the PAS cell, despite the presence of molecular sieves in the sample compartment. It is clear that the quantitative determination and qualitative analysis of these intractable drug mixtures is feasible by FTIR-PAS over the range of concentrations studied here. However, it is also apparent that, because of saturation and reflectance effects, technical improvements in the methodology (an example might be careful spectral reflectance corrections) must be introduced before very complex multicomponent solid samples can be analyzed with ease. These phenomena manifest themselves in the difficulty associated with quantitation but will be less important in qualitation.

In conclusion, the data presented here demonstrate the feasibility of rapid quantitative analysis of difficult samples (e.g. PCP on parsley) commonly encountered in the forensic laboratory. It is to be stressed that the samples are not adulterated in any way. It is therefore clear that this technique has qualitative and quantitative analytical capabilities. In addition to finding use in the forensic laboratory, it may find use wherever quantitation of solid mixtures is required such as in the analysis of food additives or pharmaceuticals and pesticides on grains.

Carbon Surfaces

There are very few convenient methods for the purification of large quantities of water or air that do not rely upon activated carbon black or activated charcoal. Thus, it is not surprising that most water treatment facilities use filter beds which contain some form of activated carbon. Similarly, most of the industrial and military gas masks use activated carbon (59), and the development of protective clothing is based upon the incorporation of activated carbon in some form of polyolefin based yarn (60). While the use of other sorbents is not uncommon (61), the most widely used absorbent in commercial and military applications is activated carbon (62). It is, therefore, very important to improve the understanding of the activation, deactivation, and function of the activated carbon.

Before any definite statements can be made about the activation, deactivation, or function of activated carbons, the surface of the carbon blacks or activated carbons, and their structure must be characterized.. Figures 31 and 32 illustrate the structures of graphite and turbostratic carbon blacks, respectively (63). Examination of these two lattice structures indicate that carbon blacks should have infrared peaks which are also present in graphite. The spectrum of lampblack, a carbon black, is shown in Figure 33. The peaks located at 800 cm^{-1} and 1500 cm^{-1} are associated with the graphite-like structure. The peak at 800 cm^{-1} is associated with the C-H out of plane bending of the graphite, whereas the peak at 1500 cm^{-1} is the ν_3 graphite peak. The other features below 2000 cm^{-1} are all due to various types of C-O stretches and bends. The band at 1750 cm^{-1} is due to C=O; the band at 1600 cm^{-1} is probably due to conjugated quinonelike carbonyls; and the

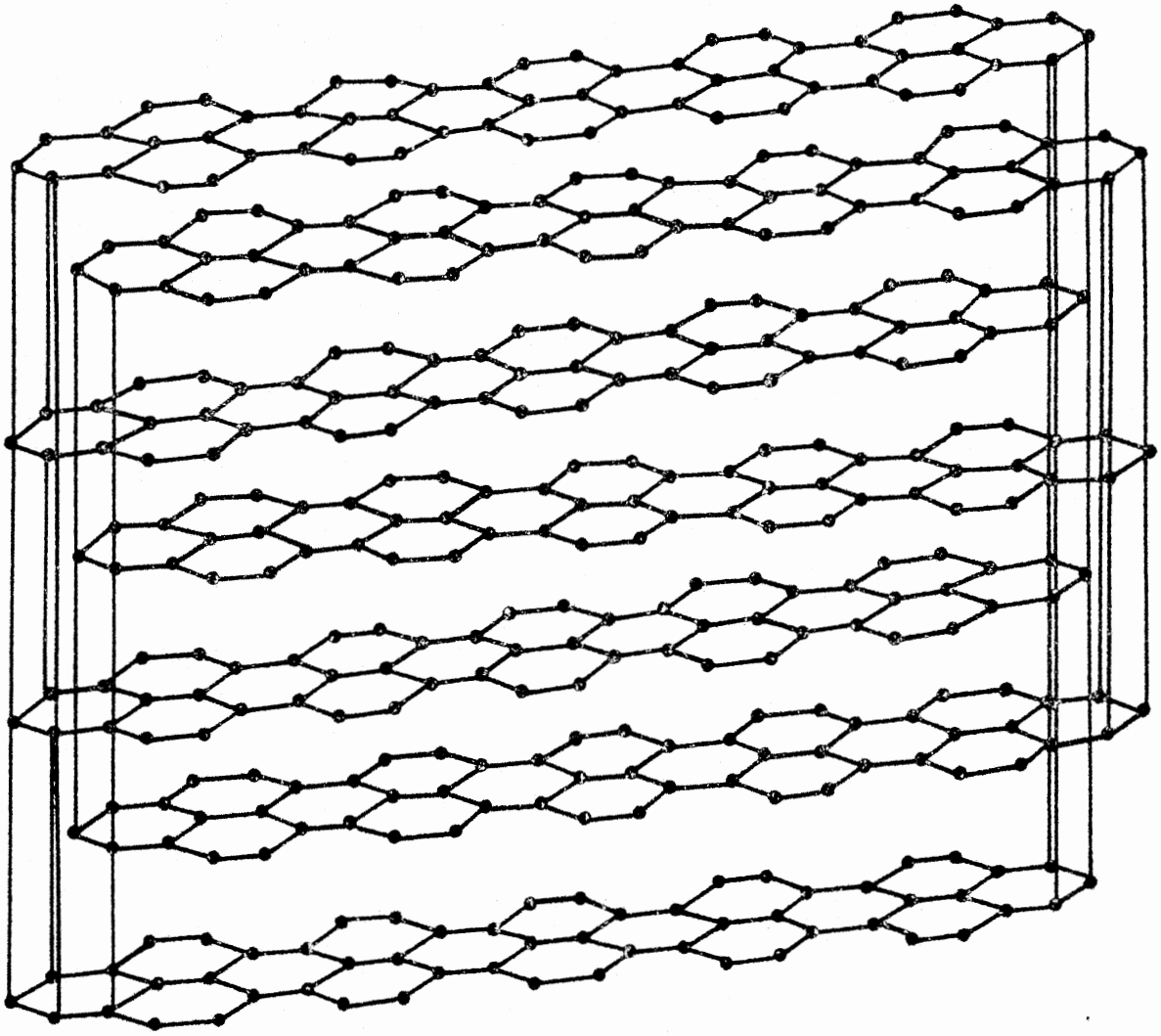

Figure 31. Schematic Diagram of the Three Dimensional Graphite Lattice

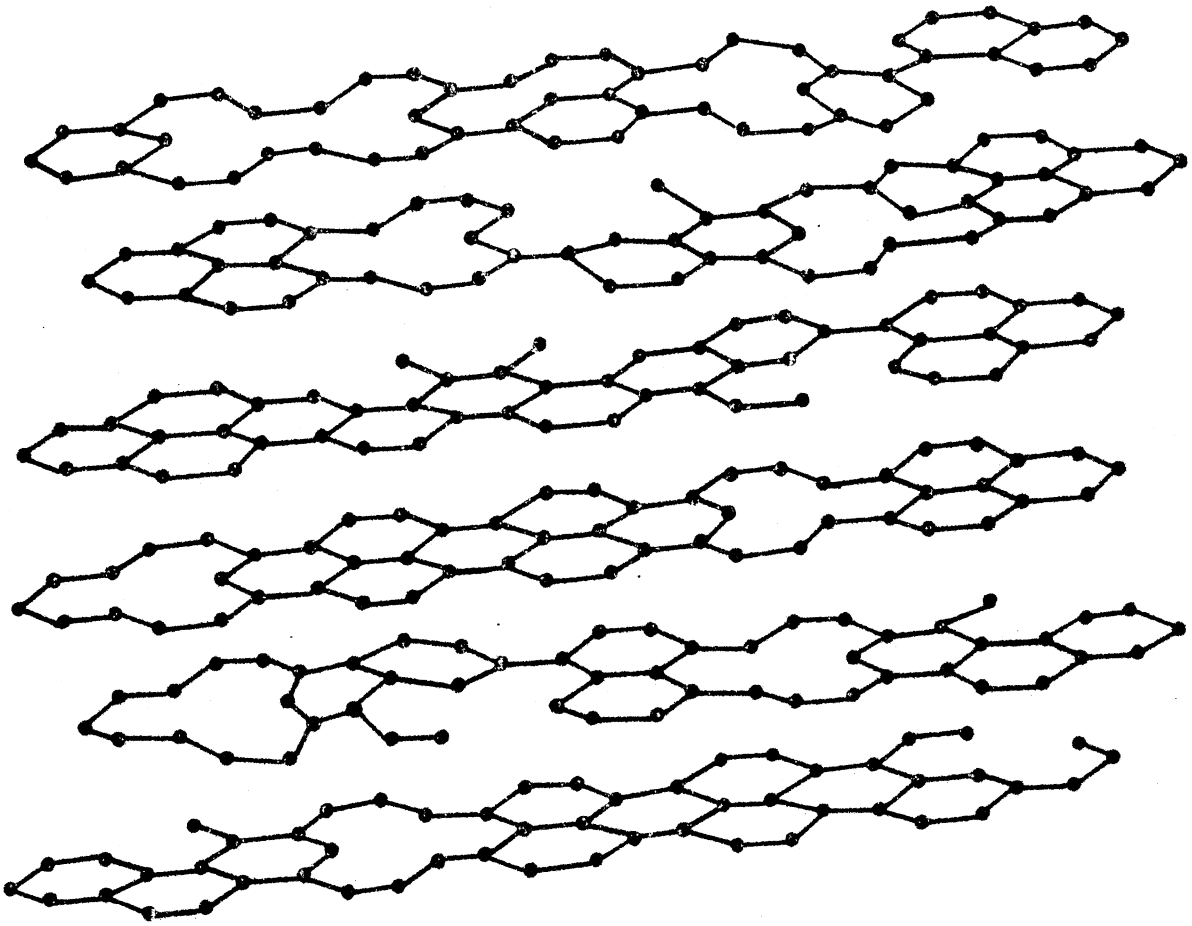

Figure 32. Schematic Diagram of the Three-Dimensional Turbostratic Structure of Carbon Blacks

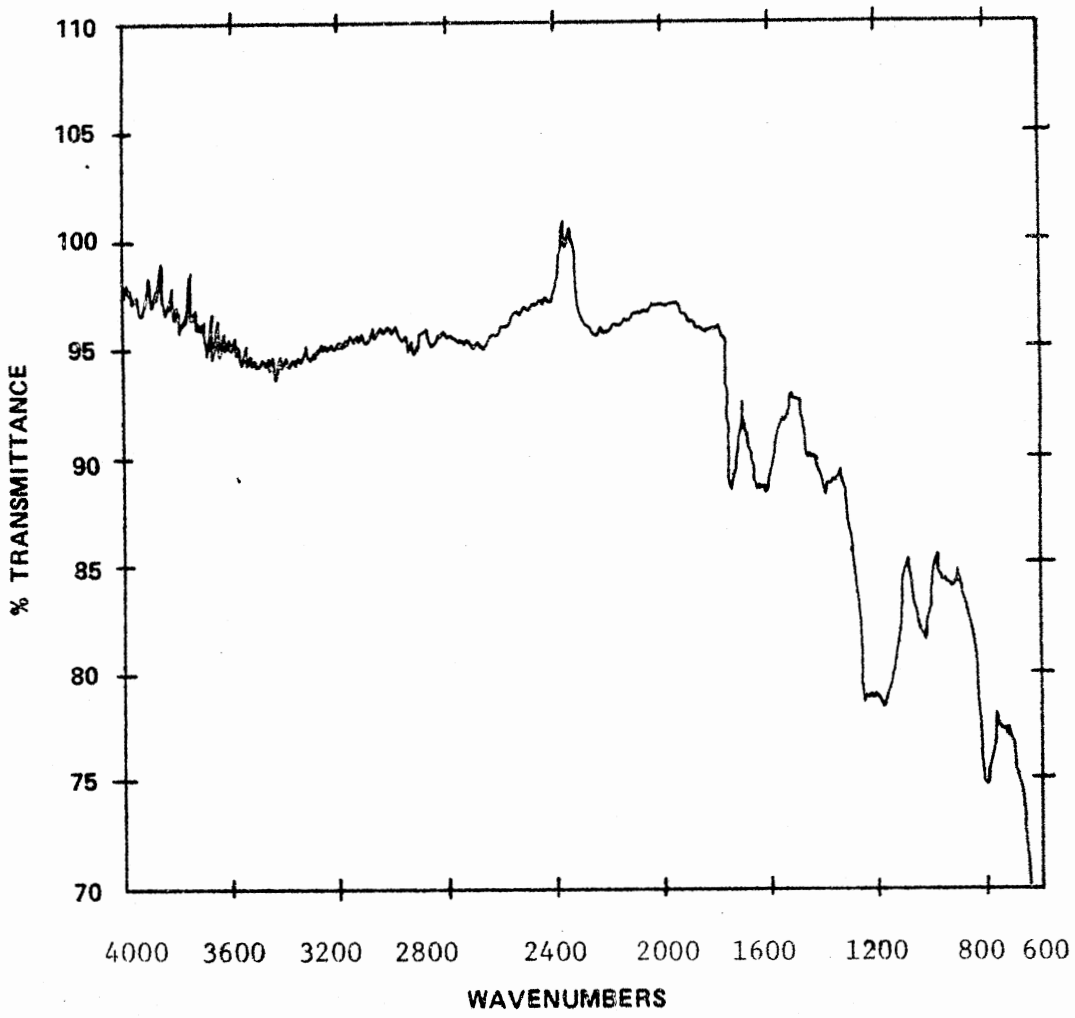

Figure 33. Photoacoustic Spectrum of Dried Lampblack

broad band from 1150-1415 cm^{-1} is attributed to aromatic C-O. The surface C-O groups are abundant if the number of lattice imperfections is high. This results in many possibilities for reactions of the edge carbons with their surroundings. This surrounding is normally air when the carbon black is formed, and thus the carbon and oxygen may readily react, with the type of carbon-oxygen group being related to the size of the imperfection.

Smith and coworkers (64) used Fourier transform infrared spectroscopy, in the 4000-1200 cm^{-1} region, to characterize an elementalcarbon surface. This surface was generated by the combustion of hexane. Smith found infrared bands at 3040, 1590, 1440 and 1260 cm^{-1}, and a complex absorption band in the 1700-1800 cm^{-1}, the relative intensities of these bands depending upon the conditions of the sample collection. Using thermal desorption studies, Smith assigned the 1590 cm^{-1} band to a carbonyl in conjugation with an aromatic ring system, while the complex absorption in the 1700-1800 cm^{-1} region is assigned to an alkyl carbonyl group and cyclic anhydride. The 3040 cm^{-1} and 1440 cm^{-1} bands were not observed when strongly oxidizing flames were used to prepare the surface and they always appeared together. Using this evidence, Smith assigned the bands to the stretching and bending modes of aromatic = C-H.

Comparison of the work on hexane soot and lampblack reveals similarities in the spectra. These similarities are to be expected because the structures of the elemental carbon surfaces are similar. The differences are due to the differences in surface generation and environment to which they have been exposed.

In order to study the interaction of carbon black with an organic chemical system, the interaction of an aqueous solution of para-

nitrophenol and carbon black was chosen. This system was chosen because it had previously been studied by Mattson and coworkers (65-67), and Friedel and Hofer (68), and thus seemed a logical place to start. Having obtained a spectrum of the carbon black, the next step was to run the spectrum of pure para-nitrophenol, shown in Figure 34, for comparison with spectra to be obtained later. In the para-nitrophenol spectrum, the most important features are the O-H stretching band from 3600-3000 cm^{-1}, the NO_2 asymmetric stretch around 1524 cm^{-1}, and the NO_2 symmetric stretch around 1360 cm^{-1}.

The first mixture run consisted of a solution of para-nitrophenol in water a concentration of approximately 0.050 moles per liter. This solution was then mixed with about one gram of lampblack. After the mixture was allowed to dry, the infrared spectrum was obtained. This spectrum is shown in Figure 35. In this spectrum, the NO_2 stretching bands have been shifted by approximately 25 cm^{-1}; the symmetric stretching band is now around 1340 cm^{-1}, and the asymmetric stretching band is now around 1500 cm^{-1}. In addition to this, the carbon black peak at around 1200 cm^{-1}, the broad C-O peak, now has strong peak at 1210 cm^{-1}. This peak is probably due to an interaction between the surface carbonyl groups and the phenolic O-H group of the para-nitrophenol. This results in the lowering of the energy of transition for the NO_2 group. It is also important to note the narrowing of the O-H peak in para-nitrophenol as the environment changes from that conducive to association of the O-H groups to that which isolates the O-H groups. This peak is somewhat broader than that normally seen for isolated O-H groups, because the interaction of the O-H surface carbonyls is most probably hydrogen bonding.

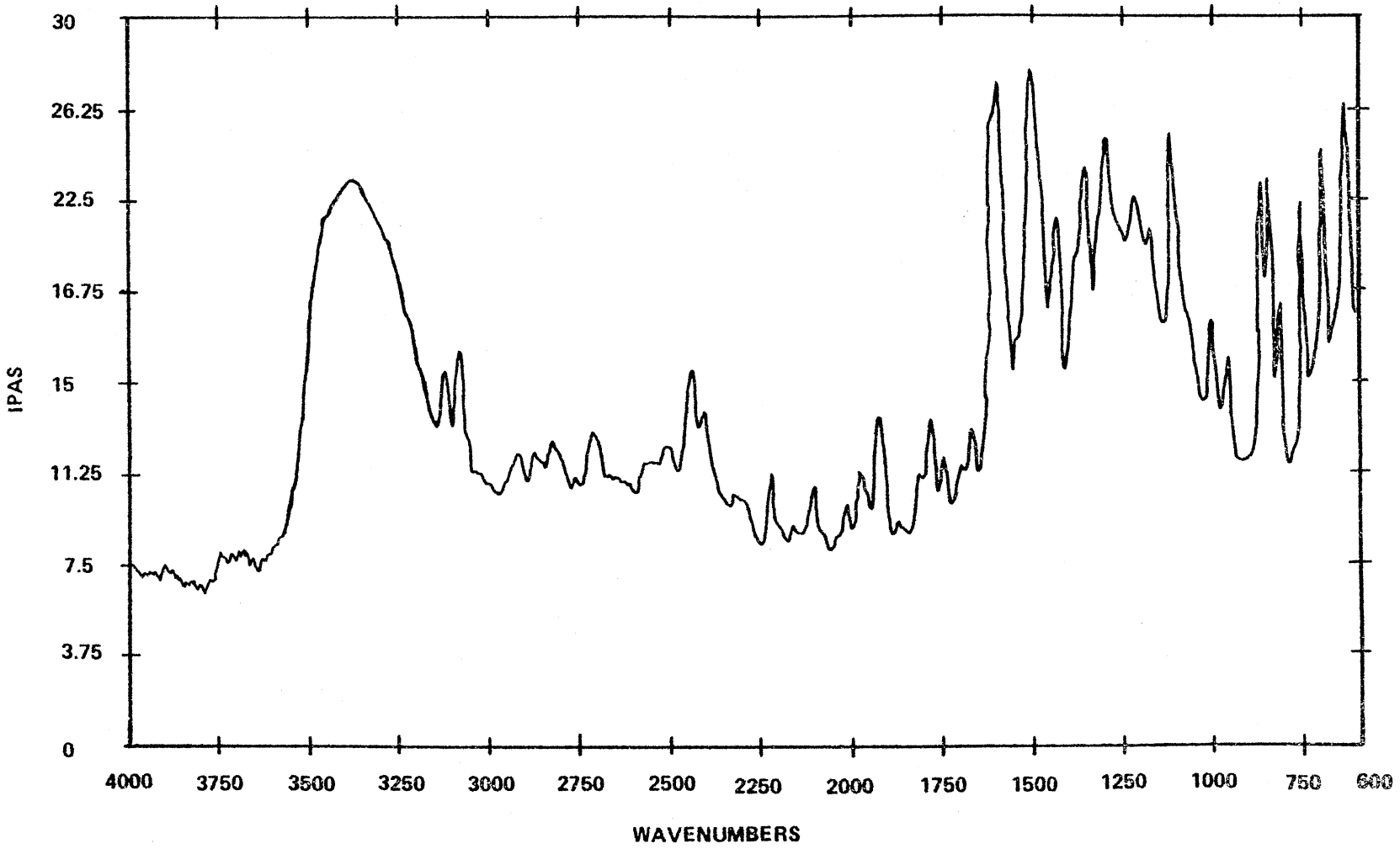

Figure 34. Photoacoustic Spectrum of Pure Para-Nitrophenol

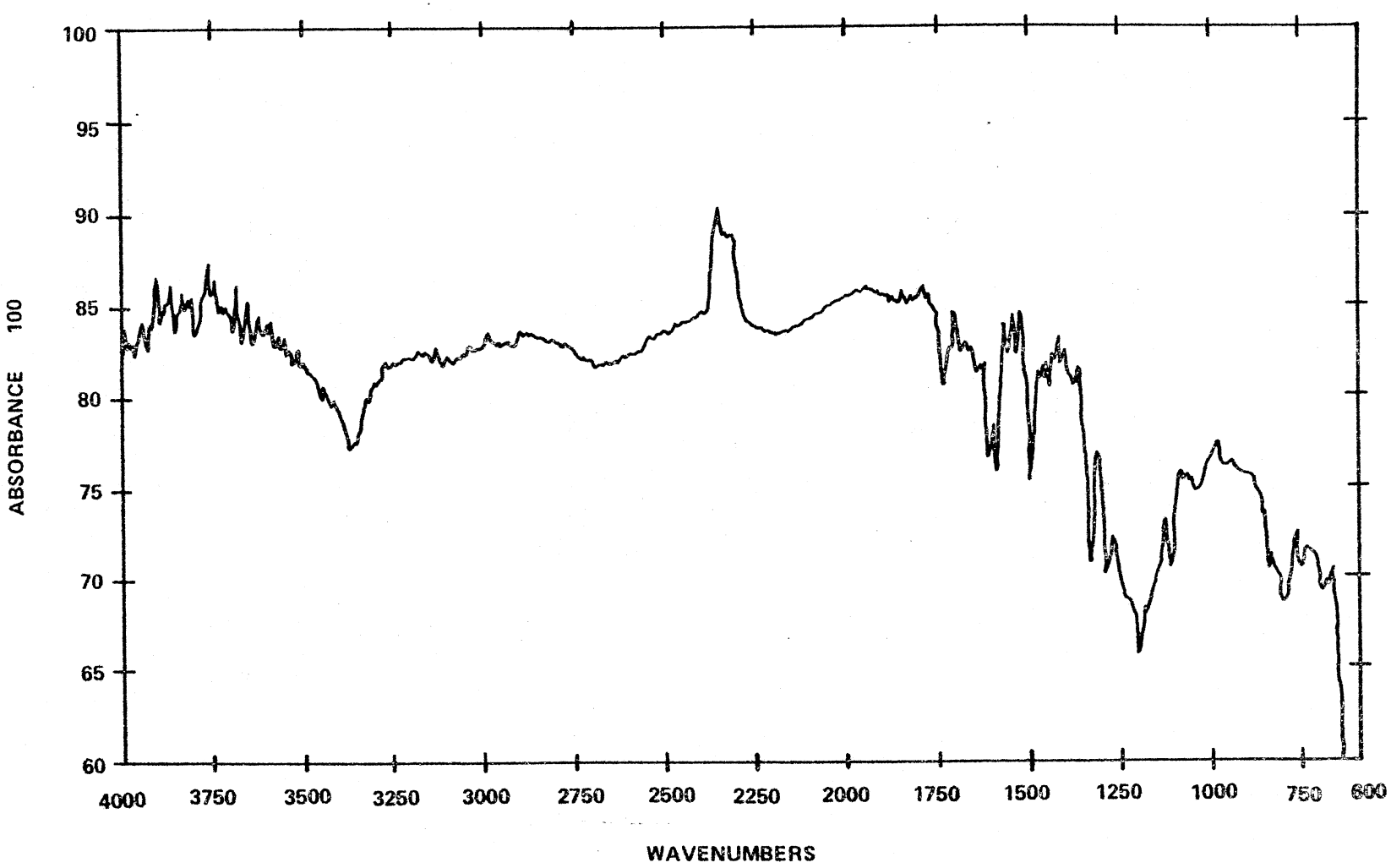

Figure 35. Photoacoustic Spectrum of Para-Nitrophenol on Lampblack

Conclusion

The studies outlined above demonstrate only a few that are possible with FTIR-PAS. Some of the studies, the analysis of biological materials, the analysis of particle size, and the analysis of the isotopic mixtures, demonstrate some of the properties of FTIR-PAS. These properties are as follows: (1) FTIR-PAS gives good qualitative information on samples with little or no sample preparations, (2) the FTIR-PAS signal may be enhanced by decreasing the particle size, and (3) FTIR-PAS may be used to perform quantitative analysis on samples. Having demonstrated the properties of FTIR-PAS, a variety of studies were performed to illustrate some of the potential uses of the technique. These studies were the analysis of carbon surfaces, a study the Department of the Army is interested in, and the forensic analysis. With these studies, the usefulness of the technique has been expanded and outlined.

SELECTED BIBLIOGRAPHY

1. Wendlandt, W.W. and Hecht, H.G., Reflectance Spectroscopy, New York: John Wiley and Sons, Inc., 1966.
2. Wilks, P.A., Jr. and Hirschfeld, T., Appl. Spectrosc., 1, 99(1968).
3. Light Scattering of Solids. Ed. G.B. Wright. New York: Springer-Verlag, 1969.
4. Rosencwaig, A., Opt. Commun., 7, 305(1973).
5. Bell, A.G., Am. J. Sci., 20, 305(1880).
6. Bell, A.G., Philos. Mag., 11(5), 510(1881).
7. Tyndall, J., Proc. R. Soc. Lond., 31, 307(1881).
8. Roentgen, W.C., Philos. Mag., 11(5), 308(1881).
9. Rayleigh, Lord, Nature, 23, 274(1881).
10. Mercadier, M.E., C.R. Hebd. Serv. Acad. Sci., 92, 409(1881).
11. Preece, W.H., Proc. R. Soc. Lond., 31, 506(1881).
12. Viengerov, M.L., Dokl. Akad. Nauk. SSSR, 19, 667(1938).
13. Pfund, A.H., Science, 90, 326(1939).
14. Luft, K.F., Z. Tech. Phys., 24, 97(1943).
15. Kruezer, L.B., J. Appl. Phys., 42, 2934(1971).
16. Kruezer, L.B. and Patel, C.K.N., Science, 173, 45(1971).
17. Parker J.G., Appl. Opt., 12, 2974(1973).
18. Rosencwaig, A. and Gersho, A., Science, 190, 556(1975).
19. Rosencwaig, A. and Gersho, A., J. Appl. Phys., 47, 64(1976).
20. Rosencwaig, A., Photoacoustics and Photoacoustic Spectroscopy, New York: John Wiley and Sons, Inc., 1980.
21. Bennett, H.S. and Forman, R.A., Appl. Opt., 15, 2405(1976).

22. Aamodt, L.C., Murphy, J.C., Parker, J.G., Appl. Phys., 48, 927(1977).

23. Wetsel, G.C. Jr. and MacDonald, F.A., Appl. Phys. Lett., 30, 252 (1977).

24. Farrow, M.M., Burnham, R.K., Eyring, E.M., Appl. Phys. Lett., 33, 735(1978).

25. Farrow, M.M., Lloyd, L.B., Risenman, S.M., Burnham, R.K., Eyring, E.M., Rev. Sci. Instrum., 51(11), 1488(1980).

26. Farrow, M.M., Lloyd, L.B., Burnham, R.K., Chandler, L.L., Eyring, E.M., Anal. Chem., 52, 1595(1980).

27. Busse, G. and Bullemer, B., Infrared Physics, 18, 255(1978).

28. Low, M.J.D. and Parodi, G.A., Appl. Spectrosc., 34, 76(1980).

29. Low, M.J.D. and Parodi, G.A., Spectrosc. Lett., 11, 581(1978).

30. Low, M.J.D. and Parodi, G.A., J. Molec. Struct., 61, 119(1980).

31. Low, M.J.D. and Parodi, G.A., Photoacoustic Spectroscopy in the Infrared Range, paper ThAb-1, "Photoacoustic Spectroscopy", digest of papers presented at the Topical Meeting on Photoacoustic Spectroscopy, Gt. Soc. Amer., Washington, DC 1979.

32. Nordal, P.E. and Kanstad, S.O., Opt. Commun., 24, 95(1978).

33. Nordal, P.E. and Kanstad, S.O., Opt. Commun., 24, 185(1978).

34. Nordal, P.E. and Kanstad, S.O., Opt. Commun., 26, 367(1978).

35. Rockley, M.G., Chem. Phys. Lett., 68, 455(1979).

36. Rockley, M.G., Appl. Spectrosc., 34, 405(1980).

37. Rockley, M.G. and Devlin, J.P., Appl. Spectrosc., 34, 407(1980).

38. Rockley, M.G., FTS/IR Notes No. 32 (Digilab, Cambridge, Mass.,1980).

39. Vidrine, D.W., Appl. Spectrosc., 34, 314(1980).

40. Rosencwaig, A., J. Appl. Phys., 52(1), 503(1981).

41. Boucher, L.J. and Katz, J.J., J.A.C.S., 89, 1340(1978).

42. Spectrum No. 8725K, Sadtler Research Lab, Catalog, (1967).

43. Koenig, J.L. and Tabb, D.L., NATO Advanced Institute Series, Series C., 57 Anal. Appl. FT-IR Mol. Biol. Syst. , 241 (1980).

44. Monchalin, J.P., Gagne, J.L., Bertrand, L., Appl. Phys. Lett.,35 360(1977).

45. Gasden, J.P. and Smith, W.L., Atm. Env., 4, 667(1970).

46. Rayleigh, Lord, Proc. Roy. Soc., A84, 25(1911).

47. Hair, M., Infrared Spectroscopy in Surface Chemistry, New York: Marcel Dekker, 1967.

48. Duyckaerts, G., Analysist, 84, 201(1959).

49. Griffiths, P.R. and Fuller, M.P., Anal. Chem., 50(13), 1905(1978).

50. Clarke, E.G.C., Isolation and Identification of Drugs, Vol. 1, London: The Pharmaceutical Press, 1978.

51. Bowen, J.M., Crone, T.A., Head, Vol., McMorrow, H.A., Kennedy, P.K., Purdie, N., J. Forensic Sci., 26(4), 664(1981).

52. Optoacoustic Spectroscopy and Detection, Ed. Y.-H. Pao, New York: Academic Press, 1977.

53. Low, M.J.D. and Parodi, G.A., Infrared Physics, 20, 333(1980).

54. Low, M.J.D. and Parodi, G.A., Spectrosc. Lett., 13, 663(1980).

55. Laufer, G., Huneke, J.T., Royce, B.S.H., Teng, Y.C., Appl. Phys. Lett., 37, 617(1980).

56. Krishnan, K., Appl. Spectrosc., 35, 549(1981).

57. Teng, Y.C. and Royce, B.S.H., Appl. Opt., 21, 77(1982).

58. Riseman, S.M. and Eyring, E.M., Spectrosc. Lett., 14(3), 163(1981).

59. Juhola, A.J. and Friel, J.V., Contract DOT-CG-64559 A, 1977.

60. Coplon, M.J. and Lapatin, G., Contract DAAG17-76-C-0085, 1977.

61. Jonas, L.A. and Eskow, J.M., Report No. EC-TR-76017, 1976.

62. Cavagnara, D.M., Order No. NTIS/PS-78/1296, 1978.

63. Mattson, J.S. and Mark, H.B., Jr., Activated Carbon, New York: Marcel Dekker, Inc., 1971.

64. Keifer, J.R., Novicky, M., Akhter, M.S., Chughtai, A.R., Smith, D.M., SPIE, 289(Fourier Transform Infrared Spectroscopy), 184(1981).

65. Mattson, J.S., Mark, H.B., Jr. Malbin, M.D., Weber, W.J., Crittenden, J.C., J. Colloid Interface Sci., 31, 116(1969).

66. Mattson, J.S, and Mark, H.B., Jr., J. Colloid Interface Sci., 31, 131(1969).

67. Mattson, J.S. and Mark, H.B., Jr., Anal. Chem., 41, 355(1969).

68. Friedel, R.A. and Hofer, J.J.E., J. Phys. Chem., 74(15), 2921(1970).

APPENDIX

TABLE I

DETERMINATION OF RELATIVE I_{PAS} OF $K^{15}NO_3$

$K^{14}NO_3$ peak height (cm)	$K^{15}NO_3$ peak height (cm)	rel. I_{PAS} $K^{15}NO_3$ (exp.)
7.35	2.50	.25
8.00	4.85	.38
5.10	6.25	.55
4.95	3.50	.41
4.90	6.85	.58
7.45	3.45	.32
5.90	10.5	.64
11.3	3.00	.21
2.20	4.60	.68
3.80	7.00	.65
2.70	9.25	.77

TABLE II

$\%K^{15}NO_3$ VS. RELATIVE I_{PAS} OF $K^{15}NO_3$

rel. I_{PAS} $K^{15}NO_3$ (exp.)	rel. I_{PAS} $K^{15}NO_3$ (calc.)	% $K^{15}NO_3$
.25	.27	0.000
.38	.38	.196
.55	.58	.469
.41	.47	.298
.58	.59	.500
.32	.33	.114
.64	.64	.600
.21	.24	.001
.68	.61	.550
.95	.95	1.000
.65	.71	.777
.77	.79	.895
slope .650 (exp.)	slope .640 (calc.)	
corr. .977 (exp.)	corr. .992 (calc.)	

TABLE III

I_{PAS} OF SiO_2 PARTICLE SIZE IN MICRONS

SiO_2 peak height/baseline	rel. I_{PAS} SiO_2 (exp.)	particle size (micrometers)
41.3/33.5	.23	55-60
56.8/28.6	.99	10-15
33.0/22.3	.48	30-35
74.0/14.0	4.29	0-5
52.0/35.5	.46	20-25

TABLE IV

ANALYSIS OF PHENOBARBITAL

SAMPLE	CALCULATED	GIVEN %
1	8.4	7.48
2	19.2	19.84
3	26.7	27.09
4	40.8	40.68
5	36.8	37.14
U1	12.0	12.34
U2	10.8	9.86
U2	10.0	9.86
U3	11.3	12.31
U3	12.8	12.31

Calculated (by FTIR-PAS) and given weight percentages of phenobarbital in lactose. U1-U3 are "unknown" with typical precisions of independent measurements of the same sample as indicated.

TABLE V

PCP ANALYSIS

SAMPLE	GIVEN %	CALC. %
1	4.1	3.97
2	9.7	9.62
3	7.1	7.15
5	3.3	3.36
6	12.2	12.24
U1	14.9	13.78
U2	6.0	8.80
U4	17.9	14.46

Calculated (by FTIR-PAS) and given weight percentages of PCP on parsley. Typical sample weights were about 10 mg

VITA 2

Dennis Michael Davis

Candidate for the Degree of

Doctor of Philosophy

Thesis: FOURIER TRANSFORM INFRARED PHOTOACOUSTIC SPECTROSCOPY

Major Field: Chemistry

Biographical:

Personal Data: Born in Gardner, Kansas, September 17, 1957, the son of Mr. and Mrs. Delmont I. Davis, Jr.

Education: Graduated from Wichita High School South, Wichita, Kansas, in May, 1975; received Bachelor of Science degree in Chemistry from Wichita State University in May, 1979; completed requirements for the Doctor of Philosophy degree at Oklahoma State University in December, 1983.

Professional Experience: Undergraduate teaching assistant, Dept. of Chemistry, Wichita State University, 1976-79; graduate teaching assistant, Department of Chemistry, Oklahoma State University, 1979-81; graduate research assistant, Department of Chemistry, Oklahoma State University, 1981-82; research chemist, Chemical Systems Laboratory, 1982-83.